Endogenous oxygen in the extremely metal-poor planetary nebula PN G135.9+55.9

Daniel Péquignot, Yiannis G. Tsamis

A&A 430, 187–212 (2005)
DOI: 10.1051/0004-6361:20041382

Astronomy & Astrophysics

Endogenous oxygen in the extremely metal-poor planetary nebula PN G135.9+55.9

D. Péquignot and Y. G. Tsamis⋆

LUTH, Laboratoire l'Univers et ses Théories, associé au CNRS (FRE 2462) et à l'Université Paris 7,
Observatoire de Paris-Meudon, 92195 Meudon Cedex, France
e-mail: Daniel.Pequignot@obspm.fr

Received 1 June 2004 / Accepted 7 September 2004

Abstract. It is shown that, in contrast to recent claims, oxygen (and helium) may *not* be extraordinarily underabundant in the new galactic halo planetary nebula (GHPN) PN G135.9+55.9 (hereafter PN G135). Determining elemental abundances in hot, highly ionized objects such as PN G135 depends critically on a proper description of the collisional excitation of the hydrogen Balmer lines, the departure from Case B recombination of hydrogen, the underlying stellar absorption lines, the shape of the primary continuum and the ionization equilibrium of highly ionized species of both oxygen and neon. Conversely, PN G135 provides unique checks of atomic data in unusual conditions: the H I collision strengths obtained by Aggarwal et al. (1991) for $1s - n$ transitions ($3 \leq n \leq 5$) are too large, while those obtained by Anderson et al. (2002) are acceptable. Empirical collision strengths are presented for $n > 5$. Photoionization models of PN G135 that fit all available optical data can be demonstrated only for oxygen abundances $12 + \log(\mathrm{O/H}) > 7.2$ (>1/30 solar) and values 0.6 dex larger are possible, depending on the assumed C/O abundance ratio. Plausible variations in the geometry of the nebula, the primary stellar continuum and the atomic data do not alter this conclusion. The C/O ratio is less than 10 by number and Ne/O is at most solar. A satisfactory model for PN G135 can be obtained in which elemental abundances are nearly the same as those of a new detailed model for K 648, the prototypical GHPN in the old globular cluster M 15 (with $12 + \log(\mathrm{O/H}) = 7.58 \sim 1/13$ solar), although C/O may be smaller. Nonetheless, given the paucity of argon and iron in the nebula, PN G135 is likely to be a more extreme Population II object than K 648, reinforcing the idea of an endogenous origin for part of the oxygen in very metal-poor PNe. Assuming a standard H-burning post-Asymptotic Giant Branch evolution, timescale and spectroscopic considerations lead to an optimal solution, in which the distance to PN G135 is 8 kpc, the effective temperature of the nucleus slightly less than 1.3×10^5 K, its luminosity 1.4×10^{37} erg s^{-1}, its mass 0.59 $M_\odot$, the age of the ionized shell 10^4 yrs, the ionized mass 0.05 $M_\odot$ and the abundances by number (H:He:C:O:Ne) = (10^6:81 500:90:30:4.5), with C/H being rather an upper limit and O/H and Ne/H uncertain by ±0.3 and ±0.1 dex respectively. Line intensities that could be used as diagnostics of the nebular elemental abundances are provided. Detailed imaging together with ultraviolet and very deep far-red spectra of PN G135 will be essential to definitely narrow the range of acceptable parameters and help us decide whether this exceptional PN is so oxygen-poor as to possibly influence current views on stellar evolution.

Key words. stars: Population II – Galaxy: halo – ISM: planetary nebulae: general –
ISM: planetary nebulae: individual: PN G135.9+55.9 – ISM: planetary nebulae: individual: K648 (Ps 1) – atomic data

1. Introduction

The object SBS 1150+559A was first convincingly identified as a Galactic Halo Planetary Nebula (GHPN) and renamed PN G135.9+55.9 (hereafter PN G135) by Tovmassian et al. (2001). From limited spectral information, these authors guessed that its oxygen abundance was about 1/300 solar ([O/H] ∼ −2.5 in the usual notation).

The GHPN nature of PN G135 was amply confirmed in subsequent imaging, spectroscopic and modelling studies (Richer et al. 2002, R02; Tovmassian et al. 2002; Jacoby et al. 2002, J02) and kinematic studies (Richer et al. 2003). Based on the extreme weakness of [O III] λ5007 and a few other spectral features, these studies all concluded that PN G135 was by far the most oxygen-poor PN known. From their extensive photoionization model analysis, R02 obtained $5.8 < 12 + \log(\mathrm{O/H}) < 6.5$, to be compared to the current (rounded-off) solar value of 8.70 (Allende Prieto et al. 2001; Bensby et al. 2004; Asplund et al. 2004). A value of 6.93 was suggested by J02 for their "final model", but they admitted that "this is probably the most conservative model": under realistic assumptions concerning notably the abundance of unseen elements – namely, $\mathrm{C/O} \ll 23$ and $\mathrm{N/O} \ll 52$ (see Sect. 5.6.3) –, J02 did find $12 + \log(\mathrm{O/H}) \sim 6.5$ ([O/H] = −2.2), in agreement with the upper limit given by R02, and did not exclude [O/H] = −2.5, the most favoured value obtained by R02.

⋆ Peter Gruber Foundation/IAU Fellow.

That, in such conditions, PN G135 is truly extraordinary can be best realized noting that the lowest oxygen abundance ever registered for any nebular object is, to our knowledge, [O/H] ~ -1.5 (blue compact galaxy I Zw 18; e.g., Izotov et al. 1999) and the record for a PN thus far is [O/H] ~ -1.1 (K 648, alias Ps 1, in the globular cluster M 15; e.g., Howard et al. 1997; abundance essentially confirmed in a recent unpublished model by Péquignot). Thus, according to R02 and J02, O/H is one or two orders of magnitude smaller in PN G135 than in any other known PN. Inasmuch as the metallicity [Fe/H] of extreme Population II (hereafter Pop II) stars in the Galactic halo ranges from −2.5 to −5, Tovmassian et al. (2001) are at first view justified in stating that their finding "does make sense". Nonetheless an extremely small [O/H] is susceptible to impact so strongly on current ideas about PN formation as to deserve special scrutiny. Helium may be another concern in PN G135, as J02 found an He/H much lower than the currently accepted pre-Galactic value.

If the extreme chemical composition of PN G135 makes it an important new object for Astrophysics, the unique physical conditions prevailing in the nebula constitute a no less important challenge for photoionization modelling.

After reviewing the possible status of PN G135 (Sect. 2), available observational material is commented on and arguments are presented in favour of an oxygen abundance in PN G135 that may not be as small as claimed in the four above mentioned papers (Sect. 3). New photoionization models are presented in Sect. 4. Results are commented on in Sect. 5 and discussed in Sect. 6, considering both astrophysical and atomic physics aspects. A "best model" is presented in Sect. 7 together with a few illustrative examples. Conclusions appear in Sect. 8.

2. What could PN G135 be?

2.1. Initial mass of the progenitor star?

The maximum initial stellar mass in a ∼13 Gyr old globular cluster should be $\sim 0.80\,M_\odot$ (VandenBerg et al. 2000 2002) so halo stars with metallicities in the range $-2.5 < [\mathrm{Fe/H}] \leq -2$ should normally end their lives as white dwarfs (WD) of mass $\sim(0.52-0.54)\,M_\odot$ (e.g., Renzini & Fusi Pecci 1988). A $0.54\,M_\odot$ pre-WD is believed to evolve so slowly as to be totally unable to ionize any previously ejected material before it disperses ("lazy" post-Asymptotic Giant Branch − post-AGB − evolution, e.g., Iben & Renzini 1983). Solutions to this general problem of GHPNe can be sought in at least five directions.

- In some Galactic evolution scenarios, the Galactic halo is partly built up from the tidal destruction and assimilation of dwarf galaxies, a process exemplified by the recently discovered Sagittarius dwarf spheroidal galaxy (e.g., Ibata et al. 1997). Given that the nucleosynthetic history of these galaxies may differ from that of the Galaxy, relatively young stars of very low metallicity (and initial mass $>1\,M_\odot$) could conceivably exist. This is highly speculative however, as known galaxies orbiting the Milky Way do not appear to harbour exceedingly metal-poor stellar populations of age significantly less than 10 Gyr (e.g., Grebel 2000). In fact, a few PNe are found in satellite dwarf galaxies (Zijlstra & Walsh 1996), but their metallicities, as traced by their sulfur and argon abundances, appear to be *larger* than in typical Pop II stars so that there is no special difficulty in assuming that their parent stars belonged to relatively young populations and had had initial masses $>1.1\,M_\odot$. Thus an extragalactic origin for PN G135, although not excluded, would not help to explain its extreme oxygen abundance.
- The dispersion timescale of a PN shell may be much larger than one believes, perhaps as a consequence of a particularly small terminal velocity of ejection for low-metallicity AGB star envelopes (Habing et al. 1994; Willson 2000). The expansion velocity of actual PNe is typically $20-30\,\mathrm{km\,s^{-1}}$, but this large velocity results from an acceleration that may be delayed until the effective temperature $T_{\rm eff}$ of the contracting post-AGB exceeds a few 10^4 K. The fact that the initial post-AGB phase of low-mass stars may last for several 10^4 yrs or even more does not imply that the pre-PN will be dispersed before it is eventually ionized. There are examples among PNe of wildly discrepant kinematic and evolutionary timescales (e.g., McCarthy et al. 1990) that may partly reflect this delayed acceleration of an otherwise slowly expanding fossil AGB wind. Nevertheless, the timescale for a PN nucleus of mass $\leq 0.565\,M_\odot$ to evolve from $T_{\rm eff} = 2.5 \times 10^4$ K to over 10^5 K (a conservative minimum in the case of PN G135, Sect. 5) is over $3{\times}10^4$ yrs (Bloecker 1995), a value which certainly exceeds the expansion timescale of PN G135 (Richer et al. 2003). Thus the nucleus of PN G135 cannot arise from a usual Pop II halo single star.
- Alternatively, a relatively massive star may be formed late in the life of Pop II stars due to the common-envelope evolution, mass transfer and possible coalescence of a close binary system (e.g., Iben & Livio 1993). While this scenario, considered in some detail by Alves et al. (2000) for K 648 (see also Jacoby et al. 1997), is especially appealing for a PN in a globular cluster where the number density of stars is high, it offers a valuable explanation for the existence of Pop II PNe in general.
- Another way to form a PN in the course of close-binary evolution is from photoionisation by the hot evolved remnant of the shell arising from the ejection of the common envelope (Iben & Tutukov 1993). The timescale problem met by low-mass Pop II single stars can now be circumvented if the common envelope phase happened to terminate just before coalescence, at a time when the system was sufficiently compact to strip almost all of the envelope of the primary, thus shortening considerably the initial (low-$T_{\rm eff}$) post-AGB evolution. A remnant mass smaller than $0.56\,M_\odot$ could be possible in this scenario.
- Finally, the mass of a PN nucleus from a metal-poor star could be larger than stellar evolution models predict due to reduced mass loss from the envelope. This explanation is hampered by the discovery of many WDs with masses close to $0.51\,M_\odot$ in the nearby globular cluster M 4 (Richer et al. 1997; see, however, de Marchi et al. 2004) and would probably not work for, e.g., K 648 (Alves et al. 2000). Nonetheless, for *extremely*

metal-deficient stars, including first-generation Population III stars (Pop III, $Z \leq 10^{-10}$) and other "crypto-Population III" stars ($Z \leq 10^{-5}$), this possibility appears quite conceivable (e.g., Willson et al. 1996). Also, the occurence of double r/s-process enriched halo stars is best understood if AGB supernovae ("Type 1.5 SNe") could explode in the early Galaxy (Zijlstra 2004), suggesting that very metal-poor intermediate-mass stars were able to grow degenerate CO cores up to the Chandrasekhar limit.

Thus, two main options are left for the origin of PN G135: (1) a post-common-envelope Pop II close binary star or (2) a low-mass (crypto-) Pop III single star (a Pop III close binary is obviously possible as well).

2.2. Expected chemical composition of PN G135?

2.2.1. Pop II progenitor (close binary)

In the prototypical GHPN K 648 where [O/H] = −1.1 and [Fe/H] = −2.26 (metallicity of M 15; Harris 1996), there are three ways to explain why [O/Fe] = +1.1.

- The present [O/Fe] of K 648 reflects the value that prevailed when M 15 was formed. This "pristine" hypothesis is taken for granted, for example, by Howard et al. (1997).
- The progenitor of K 648 was enriched in oxygen by dredge-up prior to mass loss, so that [O/Fe] is larger in K 648 than in the envelope of main sequence stars of M 15. This "endogenous" hypothesis is envisaged by Torres-Peimbert et al. (1981), Peña et al. (1991), Garnett et al. (1993) and Dinerstein et al. (2003), among others.
- The progenitor accreted matter from a companion, which formerly was a relatively massive AGB star, whose envelope was enriched in oxygen by the third dredge-up. This "exogenous" hypothesis, which may be seen as a variant of the previous one, is motivated by the existence of very metal-poor stars such as CS 29497-030, which are strongly enriched not only in carbon, nitrogen and s-elements, but in oxygen as well (Sivarani et al. 2004).

Although [O/H] is difficult to determine in cool, extremely metal-poor stars, there is growing consensus that [O/Fe] increases with decreasing [Fe/H] and reaches asymptotically ∼+0.5 for [Fe/H] ≤ −1 in the Galactic thick disk and halo (Nissen et al. 2002; Cayrel et al. 2004; Bensby et al. 2004). These observations are in agreement with the prevailing idea that, at early times, O and Fe were both injected in the InterStellar Medium (ISM) by the explosion of massive stars. Fluctuations of O/Fe are possible, however, given that the nuclear yields from individual massive stars for α-elements (from oxygen to argon) are uncertain (e.g., Woosley & Weaver 1995). Thus, Umeda & Nomoto (2003) exhibit a peculiar Pop III supernova model with [O/Fe] = 2.8. A stochastic model for the early chemical evolution of the Galactic halo by Argast et al. (2000) suggests that homogenization takes place progressively from [Fe/H] = −2.8 to −2. Since this model includes only "minimal" hydrodynamic mixing, reasonable homogeneity should be achieved by [Fe/H] = −2.2. Importantly, Cayrel et al. (2004) found that [O/Fe] is surprisingly uniform over the range −4 < [Fe/H] < −3, with a scatter of less than 0.3 dex about [O/Fe] = +0.5. Thus the first explanation for the large [O/Fe] of K 648 appears unsubstantiated. Moreover, [S/O] and [Ar/O] are both <−1 in K 648 and some other Pop II GHPNe (e.g., Barker 1983; Dinerstein et al. 2003), so the abundances of available *heavy* α-elements are roughly in harmony with [Fe/H] in M 15. As a matter of fact, there is good evidence that [S/Fe] is quite stable, say, 0.1 < [S/Fe] < 0.4 in halo stars with [Fe/H] ≪ −1 (Ryde & Lambert 2004). The same result applies to the next "even" elements [Ca/Fe] and [Ti/Fe] (Cayrel et al. 2004). Smoothing out of yields is also indirectly confirmed down to [O/H] ∼ −1.5 ([Fe/H] ∼ −2) by studies of blue compact H II galaxies (Izotov & Thuan 1999b), in which the relative abundances of α-elements are found to be virtually independent of metallicity and close to solar. Thus several lines of evidence favour an [O/Fe] ∼ +0.5 in the ISM where the progenitor of K 648 was born; the fact that [O/Fe] ∼ +1.1 in K 648 probably indicates the presence of endogenous or accreted oxygen in the envelope of the PN precursor.

Comparing the two low-abundance PNe of the Sagittarius dwarf spheroidal galaxy, Péquignot et al. (2000) found that oxygen was probably brought up to the stellar surface together with carbon by the third dredge-up accompanying the thermal pulses of AGB stars (e.g., Iben 1995). Since K 648 is extremely rich in carbon, third dredge-up could as well be responsible for the oxygen enrichment of this PN. Alternatively, Alves et al. (2000) note that, during the common-envelope evolution of a binary, hydrodynamical disturbances will greatly favour mixing of inner material with the stellar envelope (see Livio & Socker 1988; Iben & Livio 1993), resulting in the dredge-up of oxygen and other elements.

According to many theoretical and observational studies, the third dredge-up and subsequent formation of a carbon-rich AGB envelope is most efficient in metal-poor stars (Boothroyd & Sackmann 1988) and should be at work down to initial masses of the order of 1 $M_\odot$ (e.g., Lattanzio 1989). Accordingly, third dredge-up can take place in a Pop II star inasmuch as it managed to gain mass from a companion star (coalescence?). Stellar models incorporating a semi-empirical diffusive overshoot formalism do predict that oxygen is dredged up together with carbon in low-mass low-metallicity stars (Herwig et al. 2000; "fourth dredge-up", Iben 1999). In those models, the incremental enhancement ratio $\Delta O/\Delta C$ is larger than the value ∼ 0.1 suggested by Péquignot et al. (2000), while a value close to 0.07 is obtained by Marigo (2001) in her low-mass-star model predictions for chemical yields. This constitutes more evidence that endogenous oxygen can be present in GHPNe.

2.2.2. (Crypto-) Pop III progenitor (single star)

The evolution and nucleosynthetic yields of Pop III stars have received considerable attention in recent years. Since the reviews by Castellani (2000) and Chiosi (2000), theoretical material has been published by Fujimoto et al. (2000), Marigo et al. (2001), Schlattl et al. (2001), Schlattl et al. (2002),

Siess et al. (2002) and others, revealing original aspects of the evolution of these stars. Nonetheless, the results are still affected by fundamental uncertainties in the description of convective overshoot, mass loss, *etc*., especially in the initial-mass range $0.7-0.8\,M_\odot$, which includes the stars of concern here, so these results should only be used as guidelines to help us select a scenario.

Basic requirements to obtain a PN are two-fold: (1) a copious mass loss should somehow take place (for example at the tip of the AGB) in order to build up a reasonably dense and massive shell of gas; and (2) the subsequent evolution of the "post-AGB" star (more generally, the "pre-WD") to high $T_{\rm eff}$ should be fast enough to photoionize this shell before it disperses in the ISM.

As noted in Sect. 2.1, the much reduced mass loss of $Z \sim 0$ stars may allow the stellar core to grow up to a mass $\geq 0.57\,M_\odot$, large enough to prevent the "lazy evolution" of the pre-WD, even for initial masses as low as $\sim 0.8\,M_\odot$. But then how will this gentle breeze eventually convert itself into the storm that will make up the pre-PN? Willson (2000) argues that a *pulsating* AGB star will eventually enter a regime of precipitous mass loss due to hydrodynamic processes even for small metal content of the stellar atmosphere, provided that its luminosity is large enough. The lower the heavy element content, the larger the minimum luminosity (and core mass) required to expel the envelope. Whether low-mass metal-free stars really exist and eventually reach the pulsating AGB state is, however, an open question. On the other hand, the presence of heavy elements in the atmosphere is favourable to mass loss in general.

According to recent models, it is reasonably possible that a low-mass Pop III star will manage to dredge up to its surface large amounts of carbon and nitrogen, as a consequence of (core) "He-Flash-induced Mixing" (Fujimoto et al. 2000; "HEFM", Schlattl et al. 2001). HEFM is favoured by low stellar mass, low heavy element pollution of the atmosphere, the inclusion of element diffusion and the absence of convective overshoot (Schlattl et al. 2002). Including convective overshoot (which is likely to exist on other grounds) may inhibit HEFM, but evolution then proceeds to the thermal-pulse AGB phase with again the dredge-up of large amounts of CN and, this time, a non negligible amount of oxygen. Thus, the production of oxygen and heavier elements, although problematic in these stars, is possible in some scenarios (Schlattl et al. 2002; Siess et al. 2002). Many of the most metal-poor stars are known to be nitrogen-rich carbon stars with very large [C/Fe] (Rossi et al. 1999; Christlieb et al. 2004; Marsteller et al. 2003), suggesting that dredge-up of CN can indeed take place in extremely metal-poor stars, although alternative explanations are possible (e.g., Umeda & Nomoto 2003). Observational constraints on the critically important element oxygen are not yet sufficiently strong in these stars to exclude any scenario.

Summarizing, present views about the formation of halo PNe may well imply that, for whatever initial composition of the progenitor star, be it in a close binary system or not, the nebula will contain some minimum amount of CNONe, either pristine or endogenous, but the relative proportions of these elements is highly debatable. Thus, it appears possible that, in a hypothetical (crypto-) Pop III star ending as a PN, oxygen (and a fortiori neon) could be negligibly dredged up compared to carbon and nitrogen. Moreover, the formation of a PN by pure hydrodynamic ejection of a stellar envelope essentially free from heavy elements cannot be excluded on first principles. Similarly, even though a common-envelope evolution is often believed to favour mixing of inner stellar layers with the envelope, it is difficult to exclude that a common envelope totally deprived of nucleosynthetically processed material may be ejected, causing the formation of a very oxygen-poor PN. In this context, it is important to examine the extent to which the very low O/H recently claimed for PN G135 is inescapable and whether the range of acceptable O/H can be narrowed.

3. Comments on previous works

3.1. Previous modelling

The determinant aspect of the argument presented by R02 can be stated as follows. Given that [Ne III] is detected and [Ne V] is not, an upper limit exists for the intensity ratio [Ne V]/[Ne III], which can translate into an upper limit for the ionization of oxygen or else a maximum ionization correction factor $N(O)/N(O^{2+})$, that is, a maximum oxygen abundance.

Unfortunately there may be an observational weakness in this reasoning. The [Ne III]λ 3869 line is very weak and is correctly presented in Table 2 of R02 as a "2-σ detection", which means that a lower limit to the actual flux of [Ne III] can hardly be ascertained (e.g., Rola & Pelat 1994). In addition, the spectrum shown in Fig. 1 of R02 presents a steep, unphysical rise of the continuum toward the UV, precisely in the wavelength range including [Ne V]$\lambda\lambda$ 3426, 3346. The origin of this feature is not clear but the upper limit obtained for [Ne V] is doubtful.

Meanwhile, J02 obtained a new spectrum that superseded the one of R02 in the UV and showed with good signal-to-noise ratio the [Ne V] lines with the λ 3426 line having a flux 10 times stronger than the upper limit given by R02. In retrospect, one may wonder whether the steep rise in the spectrum taken by R02 was not somehow due to the [Ne V] lines themselves.

Surprisingly, J02 provided a flux for [Ne III]λ 3869 which is again about 10 *times* the one given by R02, *but again in the form of a 2-σ detection*. Agreement is good between R02 and J02 for all other lines of the spectrum. Obviously there is a problem of interpretation. In the spectrum presented by J02, a kind of a "P-Cygni bump" (artifact or stellar feature?) appears to the blue of [Ne III]λ 3869, at 3850 Å. Presumably J02 adopted a large value on the basis of the size of the bump, but attached such a large error to the line flux as to make the very detection of [Ne III] uncertain. Nonetheless a tiny line can be guessed in that spectrum at the expected wavelength of [Ne III] and correctly pointed out by the authors. On close inspection of both spectra, it is quite probable that [Ne III] is weak, with a flux not exceeding much the one given by R02. Note that the prospect for a relatively large [Ne III]λ 3869 flux, as suggested by J02, is jeopardized by the weakness of the line at 3970 Å, which should be a blend of [Ne III]λ 3969 (intensity 31% of [Ne III]λ 3869; Mendoza 1983) with H7 λ 3970: even after correcting for the Ca II interstellar absorption line, the observed intensity of λ 3970 tends to be somewhat weaker than the value

Table 1. H I and He II lines in PN G135.

Observations and corrections	Hα 6562.8	Hβ 4861.3	Hγ 4340.5	Hδ 4101.7	H7 3970.1	H8 3889.0	H9 3835.4	He II 4685.7	He II 5411.6
$\langle SPM(R02)\rangle$	294.0 ± 16	100. ± 0.0	41.9 ± 1.4	20.7 ± 1.0	6.4 ± 2.5	–	–	79.4 ± 2.5	5.5 ± 0.2
Median (R02)	292.4	100.	41.5	20.9	5.5	–	–	77.	5.5
MMT (J02)	289.7 ± 10	100. ± 0	38.4 ± 3	16.7 ± 2	3.9 ± 1	–	–	73.0 ± 3	5.3 ± 1
CFHT (R02)	260.3 ± 5.	100. ± 0.0	42.1 ± 1.0	20.6 ± 1.2	6.11 ± 0.6	2.92 ± 0.7	0.00 ± 0.7	78.6 ± 1.5	5.23 ± 0.3
CFHT de-redd.	287.7 ± 15[a]	100. ± 0.0	42.5 ± 1.0	20.8 ± 1.2	6.18 ± 0.6	2.95 ± 0.7	0.00 ± 0.7	78.8 ± 1.5	5.18 ± 0.3
I(Case B)	270.0	(100.)	47.8	26.6	16.4	10.8	7.5	(78.8)	6.39
$I_{\rm theo}$ approx.	∼277.	100.	∼45.6	∼24.2	∼14.7	∼9.6	∼6.6	78.8	∼6.41
Cont./Å/$I_{\rm H\beta}$	1/209.2	1/65.3	1/43.1	1/33.7	1/29.8	1/27.5	1/26.0	1/56.6	1/99.0
EW(Å) $I_{\rm theo}$	580.0	65.3	19.6	8.16	4.38	2.64	1.72	44.6	7.78
EW(Å) – 1.8 Å	578.2	63.5	17.8	6.36	2.58	0.84	−0.084	42.8	5.98
$\delta(I_{\rm theo})$	7.0	0.0	−3.0	−4.8	−5.8	−6.46	−6.63	−1.04	−1.34
CFHT – $\delta(I_{\rm theo})$	280.7	100.	45.5	25.6	12.0[b]	9.41	6.63	79.8	6.52

[a] From average of SPM spectra (Sect. 3.2.2).
[b] Intensity between 12.4 and 13.5 after correcting for Ca II absorption (Sect. 3.2.2).

expected for H7 (interpolating between adjacent Balmer lines in Table 1, see Sect. 3.2.2) and [Ne III] should not significantly contribute to the blend.

It can now be understood why J02 found an oxygen abundance nearly equal to the upper boundary of the range accepted by R02, namely [O/H] ∼ −2.2. It happens that, (1) the [Ne V] flux measured by J02 is about 10 times the upper limit claimed by R02; and (2) the [Ne III] flux *assumed* by J02 is also about 10 times the one *assumed* by R02. Then the [Ne V]/[Ne III] ratio adopted by J02 nearly coincides with the upper limit accepted by R02 and this upper limit corresponds to the upper boundary for [O/H]. However, as just noted for the data secured by R02, but in a much exacerbated manner, J02 are *not* well-founded to take their indicative flux for [Ne III] for granted since this is fundamentally unreliable. In fact it is reasonably probable that the actual [Ne III] flux is at least 1.0 dex smaller than the value adopted by J02.

In summary, collecting together the data secured by R02 and J02, the spectrum of PN G135 includes (1) a very weak [O III]; (2) a strong [Ne V]; and (3) a stringent upper limit on [Ne III] (this limit will be taken as 1.5 times the best value obtained by R02). It follows that the original argument of R02 is now exactly *inverted*. Setting the maximum possible value to the flux of [Ne III] implies that [Ne V]/[Ne III] is a *lower limit*, not an upper one, and there exists a *lower boundary* to the oxygen abundance. Thus, *it is no more necessarily true that [O/H] should be exceptionally small in PN G135*. New modelling is in order to reset boundaries on the oxygen abundance of PN G135.

3.2. Spectroscopic observations

3.2.1. Available data

A Multi-Mirror Telescope (MMT+FLWO) optical spectrum was secured by J02. One Canada-France-Hawai Telescope (CFHT) and four different San Pedro Martir (SPM) spectra were secured by R02 in the optical, complemented with a deep far-red William Herschel Telescope (WHT) spectrum. Except for the [Ne V] lines taken from J02, the CFHT observations are generally preferred as they were obtained through a slit encompassing most of the nebula, they are deeper and more comprehensive.

According to R02, the 2-σ upper limit flux for undetected lines is typically <1.0 ($I_{\rm H\beta}$ = 100) in the optical CFHT spectrum, with a value as low as 0.3 at 5876 Å, whereas in the WHT spectrum (λ > 6820 Å) the upper limits are quoted as substancially <0.1. The line-flux upper limits noted by R02 deal with relatively low-ionization species that may not be the most constraining for this high-ionization object, Relevant lines include [Ne IV]$\lambda\lambda$ 4714, 4725, [Ar V]$\lambda\lambda$ 7005, 6435, [Fe VII]λ 6087, C IVλ 4658, C IVλ 7726, N Vλ 4645, O IVλ 4632, and O IVλ 7713. We adopt upper limits of ∼1.0 in the optical, ∼0.5 in the red and ∼0.1 in the far-red for these lines. The far-red upper limits may be more tentative due to possible telluric features. As stated at the end of Sect. 3.1, the uncertain [Ne III]λ 3869 flux will be conservatively treated as an upper limit in the discussion. Although [Ne III] appears crucial in previous modellings, it will turn out to be unimportant here (Sect. 5.7).

Reddening is small for PN G135 and cannot affect conclusions. Following Schlegel et al. (1998), E_{B-V} = 0.02 is adopted (0.00 and 0.03 in R02 and J02 respectively).

3.2.2. Stellar absorption lines

In the first rows of Table 1 are listed, for the intensities of H I and He II lines in units $I_{\rm H\beta}$ = 100, (1) the average and 1-σ scatter of the SPM values listed by R02; (2) the median of these values; (3) the MMT value; and finally (4) the CFHT value. The large data set secured by R02 allows us to check that the consistency of the observations is excellent except however for Hα, whose flux is suspected by R02 to vary with time. The Hα flux appears anomalously weak in the CFHT spectrum and is multiplied here by a factor ∼1.13. The dereddened CFHT fluxes

are given in the 5th row of Table 1 and can be compared to the Case B recombination intensities (Storey & Hummer 1995), given in the 6th row, assuming $T_e = 3 \times 10^4$ K.

The Balmer decrement appears much steeper for principal quantum numbers $n > 4$ than under Case B recombination conditions. Given that the Case A and Case B decrements are about the same and that, in intermediate conditions, H8 can be depleted by at most ∼20% relative to Hβ (Hummer & Storey 1992), the fading of the Balmer lines for large n's is not mainly due to departure from Case B. Alternatively, this effect is likely to be the signature of underlying stellar H I and/or He II absorption lines. Since the stellar continuum is strongly increasing to the blue, whereas the equivalent width (*EW*) of the stellar Balmer lines is generally weakly dependent on n, the sum of the nebular and stellar lines will decrease as n increases.

*EW*s are given by R02 for the observed emission lines Hα and Hβ. Anticipating some departure from Case B (Sect. 5.5), an *approximate* theoretical Balmer decrement is guessed (row 7), from which theoretical *EW*s are computed (row 9), using the observed *EW* for Hβ (65.3 Å) and assuming a continuum $\mathcal{F}_\lambda \propto \lambda^{-3.88}$ (row 8), suited to the hot central star (the observations of R02 lead to $\mathcal{F}_\lambda^{\rm obs} \propto \lambda^{-3.93\pm0.25}$, in excellent agreement).

Subtracting an arbitrary $EW_{\rm abs}$ independent of n from these theoretical *EW*s, corrected *EW*s are obtained (row 10), that can be converted into corrected theoretical intensities, again relative to $I_{\rm H\beta} = 100$. Subtracting the difference $\delta(I_{\rm theo})$ between the corrected and initial theoretical intensities (row 11) from the observed CFHT intensities leads to observed intensities corrected for stellar absorption [noted CFHT $- \delta(I_{\rm theo})$, row 12] , that can be compared to the theoretical guess (row 7). The value 1.8 Å adopted for $EW_{\rm abs}$ in Table 1 is intended to optimize the comparison. The argument is not circular because the determination of $EW_{\rm abs}$ is very strongly weighted by the highest order Balmer lines observed, H8 and H9, whose *EW*s are $\leq EW_{\rm abs}$. Changing reasonably the theoretical guess has negligible effect on the correction to be applied to the Balmer lines of interest here.

The fact that, compared to adjacent lines, the corrected H7 intensity appears too weak in Table 1 could be partly due to absorption by the interstellar Ca II λ 3968.47 line, whose wavelength in the velocity frame of PN G135 is 3971.03 Å, that is +0.96 Å off the H7 line. Although H7 may not be significantly affected, the adjacent continuum blended with H7 at the spectral resolution of the observations will be. The statistical *EW* of the Ca II line in the direction of PN G135 is 120 mÅ (Beers 1990), resulting in an extra correction of +0.40 to the intensity provided in row 12. The maximum correction would be +1.48 if Ca II and H7 were coincident in wavelength and width.

Similarly, the theoretical intensity ratio He II(7−4)5412/ He II(4−3)4686 (almost insensitive to departure from Case B in the conditions of PN G135) is ∼3-σ off (last two columns of Table 1) and will be brought back into agreement with observation if the He II lines are corrected for an underlying absorption $EW_{\rm abs}$(He II), that turns out to be again 1.8 Å.

The aim of these corrections is to refine as much as possible the intensities of the strongest H I and He II nebular lines (Sects. 5.5, 5.6 and 7). The corrections are sufficiently small to justify the simple procedure used, yet large enough to be worthwhile.

The absolute flux of Hβ is obtained from the 5 arcsec wide CFHT slit:

$$I_{\rm neb}({\rm H}\beta) = 2.55 \times 10^{-14} \times 1.0692 \times (1.0283/1.0430) = 2.7 \times 10^{-14}\,{\rm erg\,cm^{-2}\,s^{-1}},$$

where the three correcting factors are for the reddening, the assumed underlying absorption and the He II(8−4)λ 4859 nebular emission line respectively. Similarly:

$$I_{\rm neb}({\rm He\,II}\,4686)/I_{\rm neb}({\rm H}\beta) = 0.786 \times 1.0025 \times 1.0420 \times (1.0430/1.0283) = 0.832.$$

The resulting "observed" de-reddened and corrected (nebular) spectrum, including useful upper limits and uncertainties, is provided in Cols. 3−4 of Table 4 (Sect. 7).

4. New photoionization models for PN G135

4.1. Modelling considerations

The computations were done with the code NEBU which was recently compared to other photoionization codes in standard conditions (Péquignot et al. 2001). In addition to the observed line intensities (Table 4), the models are subject to constraints on the ionizing source and the gas density distribution.

4.1.1. Central star

The optical continuum of the central star must correspond to the observed continuum. This is achieved if (1) $T_{\rm eff} > 6 \times 10^4$ K; and (2) the dereddened continuum flux at λ 5556 Å is 2.66×10^{-16} erg cm^{-2} s^{-1} Å^{-1} (R02). In most of this investigation, it will be assumed, following R02 and J02, that the central star radiates like a black body (see, however, Sect. 6.5). With this assumption, it is found that the stellar luminosity L can be related to $T_{\rm eff}$ and the distance D by the interpolation formula:

$$L = 1.61 \times 10^{37} \times (T_{\rm eff}/1.3 \times 10^5\,{\rm K})^{2.88} \times (D/10\,{\rm kpc})^2\,{\rm erg\,s^{-1}}.$$

According to stellar atmosphere models, the ionizing spectrum of hot stars presents a discontinuity at the He^+ edge and severe departures from a black body are common in the high energy tail of this spectrum (Rauch 2003). The computations are exceedingly difficult and the results depend on poorly known parameters, such as the elemental abundances. In addition, the shape of the continuum is sensitive to the presence of a stellar wind (Kudritzki & Puls 2000). Generally speaking, it is difficult to quantify the effect of unsteady, disordered, irreversible shock processes in the atmosphere of these stars, that may contribute to damp departures from the black body in the emergent spectrum.

Models based on the black-body assumption will be evaluated using stellar spectra made available by Rauch (2003). It will become apparent that, for the most important aspects of this work, black bodies lead to *more conservative* conclusions

than elaborate model atmospheres do (Sect. 6.5), providing one further justification to first consider this simplest case.

4.1.2. Ionized shell geometry

The azimuthally averaged brightness distribution results in a spherically symmetric model nebula whose radial hydrogen density profile is given by R02 as:

$n_{\rm H} = n_c \times \exp(-r/h)^2$,

with r the radius, $h = 4.19 \times 10^{17} \times (D/10\,{\rm kpc})$ cm and n_c a free parameter. The inner radius is arbitrarily taken as $r_{\rm in} = h/4$ and the outer radius as $r_{\rm out} = 1.8 \times h$ (~5 arcsec), intermediate between the values quoted by R02 and J02. Adopting a smaller $r_{\rm in}$ and/or a larger $r_{\rm out}$ has no effect on the computed line intensities of interest. Most computations were done assuming a spherical symmetry with the above density variation, a uniform chemical composition and a smooth small-scale gas density distribution, that is, a local volume filling factor unity, $fill = 1$.

According to the spatiokinematic study of Richer et al. (2003), the outward decrease of emissivity is confirmed but a prolate ellipsoidal shape is more appropriate than a spherical shape (see also J02) and the gas distribution is asymmetrical. The exact global geometry is by itself of little concern in this optically thin nebula[1], once the bulk of the gas is at the right angular distance from the star, but the asymmetry suggests that the average gas density may vary according to the radial direction. Some computations were therefore done assuming that the nebula intercepts only half the sky of the star (covering factor $f = \Omega/4\pi = 0.5$). In the thin case, this is equivalent to assuming $fill = 0.5$ with full coverage of the ionizing source.

4.2. Departure from Case B recombination

The small column density of neutral hydrogen in the highly ionized, strongly matter-bounded PN G135 may result in a departure from Case B recombination of the Balmer lines (Hummer & Storey 1992). Similarly the abundance of helium relies on He II and the column density of He^+ is not very large either.

Solving the full transfer and cascade matrix of the hydrogenic ions is out of the scope of the code NEBU and self-consistent, but approximate treatments prove to meet difficulties at recovering exact detailed solutions. Here, computations of the H I and He II recombination emissivities have been performed using either the classical Case B approximation (infinite depth of the Lyman lines) or direct fits to the accurate non-Case B results of Hummer & Storey (1992), parameterized by the Lyα optical depth. Hummer & Storey considered a uniform slab at 10^4 K, but, within reasonable limits, the results are not expected to depend much on temperature or geometry, once proper scaling laws are introduced. Here, only He II Pα (λ 4686 Å) and the first H I Balmer lines need be considered.

In practice the slab optical depth is identified with the radial optical depth of the model nebula. For covering factor $f < 1$, the optical depth will be larger. However, for $f < 0.5$, lateral leakage of photons will become dominant since the shell is not geometrically thin and the "effective optical depth" will not increase any more. Thus, considering $f = 1$ and 0.5 (Sect. 4.1.2) is a way to approximately bracket the effect of geometry on departure from Case B.

4.3. Atomic physics

Physical conditions in PN G135 are unusual among PNe and photoionized nebulae in general. Therefore atomic parameters that are normally of relatively little concern in model nebulae and may not be of ultimate accuracy can now have a serious impact on astrophysical predictions and conclusions. Conversely, spectroscopic observations of PN G135 can be of help in checking atomic data in unprecedented conditions. Two aspects are particularly noteworthy. First, the O^{2+} ionic fraction is exceedingly small, with most of the oxygen in higher ionization stages. Second, according to models, the electron temperature $T_{\rm e}$ in PN G135 may range from 2 to 4×10^4 K, resulting in the collisional excitation of hydrogen.

4.3.1. Ionization equilibrium of oxygen and neon

In most PNe, the average fractional abundance of O^{2+} is weakly dependent on the details of the ionization and recombination processes as long as an He^+ zone exists where this ion is dominant. In PN G135, the ionization fraction of O^{2+} is everywhere very small and therefore roughly proportional to the product of the recombination coefficients of O^{2+} and O^{3+} (Sect. 5.2). For lack of anything better, the recombination coefficient is often taken as the sum of the radiative (e.g., Péquignot et al. 1991) and dielectronic (Nussbaumer & Storey 1984) recombination coefficients. In the case of oxygen, Nahar (1999) performed a more comprehensive unified calculation, resulting in total recombination coefficients that tend to be *smaller* than the traditional sum by factors 1.3−2.0 in the range of $T_{\rm e}$ of interest. In NEBU calculations, the data of Nahar are normally incorporated, but questions can be raised about their accuracy until independent computations are undertaken. For example, in a detailed computation for N^+, Kisielius & Storey (2002) found a recombination coefficient somewhat larger than the one obtained by Nahar & Pradhan (1997) with methods similar to those employed by Nahar (1999). Given that Nahar's results are not necessarily incorporated in photoionization codes (e.g., in the one used by R02), some models will be computed using the more traditional (pre-Nahar) sum for comparison.

Also, the neon recombination coefficients may not be of ultimate accuracy. Since the ionization balance between Ne^{3+} and Ne^{4+} will indirectly control an important diagnostic for the oxygen abundance determination (Sect. 6.1.1), some alternative computations will be done assuming that the total recombination coefficient of Ne^{3+} is, by analogy with oxygen, divided by a factor 1.5. Doubts may be expressed about the Ne^{2+} coefficient as well, but no important diagnostic is attached to it in the present study.

[1] See however Sect. 4.2 for departure from Case B.

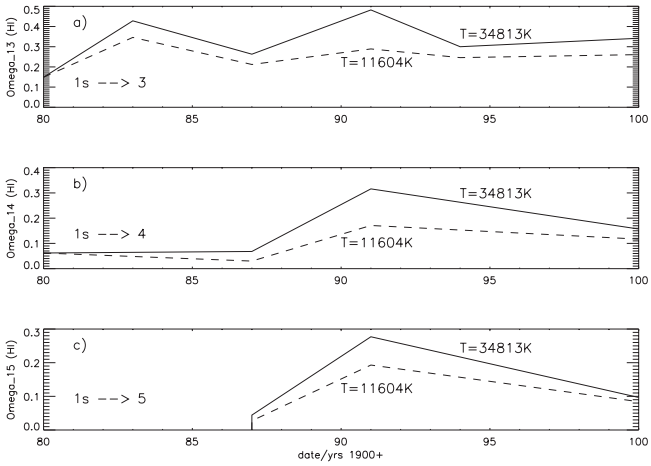

Fig. 1. Hydrogen effective collision strengths at temperatures 1 eV (T_e = 11 604 K, dashed lines) and 3 eV (T_e = 34 813 K, solid lines) for inelastic electron collisions from the ground state H I(1s) to H I(n), n = 3, 4 and 5, versus the publication date between years 1980 and 2000.

4.3.2. Collisional excitation of hydrogen

Interest in the collisional excitation of hydrogen was renewed when astronomers tried to account for the H I spectrum of active galactic nuclei (e.g., Krolik & McKee 1978).

Computing accurate collision strengths for the H I transitions is a notoriously difficult task and the difficulty tends to increase with increasing principal quantum number n. At the very low density of PN G135, only collisions from level 1s need be considered. Collisional excitation to n = 2 is an important cooling process in PN G135, but the rate is not controversial. In Fig. 1, total effective collision strengths to n = 3, 4 and 5 are shown for two temperatures versus their publication date in the years 1980–2000. Literature about this topic is considerable. Here, only some representative compilations (Drake & Ulrich 1980; Aggarwal 1983, for n = 3; Giovanardi et al. 1987; Callaway 1994) and two comprehensive computations (Aggarwal et al. 1991; and Anderson et al. 2000, both for all levels $n \leq 5$), that were effectively available for nebular studies, are considered. The plotted variations of the collision strengths since 1980 are very large. They are even larger for transitions to individual nl levels (The nl's must obviously be considered in actual model nebulae).

In the 80's and early 90's, detailed computations concentrated on low n transitions. Callaway (1994) summarized the state of the art and provided fits for transitions $n \leq 3$. For these transitions, the results of the first extensive R-matrix calculation (Aggarwal et al. 1991) were judged too large – particularly at high T_e – for having omitted channels representing continuum states. Concerning higher levels, different recipes based on semi-classical approaches, Born approximation, distorted wave approximation and semi-empirical estimates (e.g., Johnson 1972) have been in use until very recently. However Callaway (1994) also noted that the only data that had some claim to reliability for $n > 3$ were those of Aggarwal et al. (1991), which included a detailed treatment of resonances, but only for $T_e < 10^4$ K, as, in analogy with the case of n = 3, they could be overestimated at high energies. Recently, new R-matrix cross sections incorporating a consistent pseudo-state treatment of the continuum were obtained for all $n \leq 5$ transitions by Anderson et al. (2000) (see also Erratum, Anderson et al. 2002) and were indeed smaller than those published by Aggarwal et al., yet larger than early estimates.

Following the review by Callaway (1994), doubts about the R-matrix results left astronomers with different options. Such or such old result may still be in use in many codes. If it is probably fair to consider a priori these recent results as the most reliable to date, it would be premature to accept that they have reached ultimate accuracy.

Since laboratory measurements of these cross sections appear to be difficult, observational consequences of different atomic data sets in the natural laboratory offered by PN G135 may provide useful insights for other astrophysical applications. Three different sets will be considered, corresponding to possible "states of the art" in the years 1987 (Giovanardi et al. 1987), 1994 (Callaway 1994, for n = 2 and 3; Aggarwal et al. 1991, for $n > 3$), and 2002 (Anderson et al. 2002). Encoding letters G, F, and A respectively will be associated to these three sets.

5. Results

5.1. Photoionization model sequences

With the astrophysical assumptions of Sect. 4.1, for any given values of the two main free parameters D and $T_{\rm eff}$, the values of n_c, He/H, O/H and Ne/H are uniquely determined by the four available observables $I_{H\beta}$, He II λ 4686, [O III]λ 5007 and [Ne V]λ 3426. In order to fully determine a computation, a pair of secondary free parameters, namely (C/O, N/O), must also be specified as carbon and nitrogen can be important gas coolants. The heavier elements contribute negligibly to the cooling (Sect. 6.2). In practice, computations are done assuming abundances by number (H:Mg:Si:S:Cl:Ar:Ca:Fe:Ni) = (10^8:10:5:4:0.1:1:0.5:1:0.1) and any output line intensity is simply proportional to the relevant (yet reasonably small) abundance adopted.

Sequences of models parameterized by $T_5 = T_{\rm eff}/10^5$ K were obtained for distances D/kpc = 8, 10 and 15 (noted respectively D8, D10 and D15) and two pairs of (C/O, N/O) ratios, namely (1.5, 0.5) [moderate C/O, noted C1] and (7.3, 0.37) [large C/O, noted C7]. The latter pair is taken from our unpublished model of K 648. A letter – A, F or G – is attached to each sequence to specify the collision strengths used for hydrogen (Sect. 4.3.2). Index nB ("not Case B") is appended to sequences in which departure from Case B was allowed for H I and He II (Sect. 4.2).

Variant sequences were considered, in which the oxygen and neon recombination coefficients were modified (Sect. 4.3.1). A variant allowed for properties of the nebula geometry (Sect. 4.1.2). Computed model sequences are listed in Table 2. Properties of the stellar continuum are considered separately in Sect. 6.5.

Table 2. Model sequences for PN G135.

Definition[a]	D8	D10	D15	D10 variants[b]
C1A		x		f05, α(O), $\alpha(Ne^{3+})$
C7A		x		
C1F	x	x	x	
C7F		x	x	
C1G		x		
C7G		x		
C1A nB	x	x	x	f05, α(O)
C7A nB	x	x	x	f05
C7F nB		x		

[a] C1 and C7: (C, O) = (1.5, 0.5) and (7.3, 0.37); nB = not Case B; G = Giovanardi et al. (1987); F = Aggarwal et al. (1991); A = Anderson et al. (2002).
[b] f05: $f = 0.5$; α(O): pre-Nahar coeffs.; $\alpha(Ne^{3+})$: coeff. / 1.5.

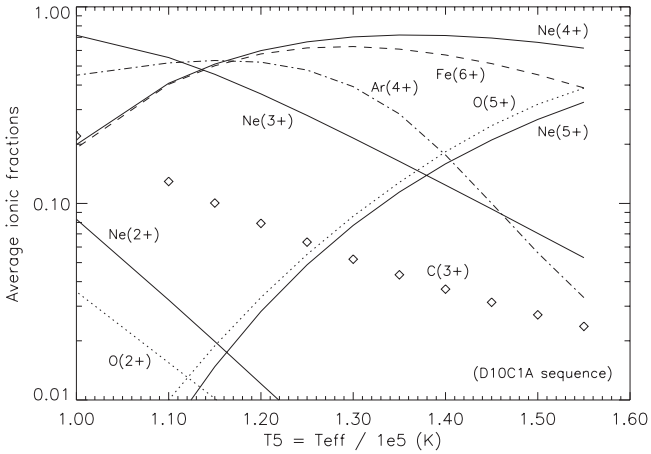

Fig. 2. Average ionic fractions versus $T_5 = T_{\rm eff}/10^5$ K for ions Ne^{2+}–Ne^{5+} (solid lines), O^{2+}, O^{5+} (dotted lines), C^{3+} (diamonds), Ar^{4+} (dash-dotted line) and Fe^{6+} (dashed line) in D10C1A models.

5.2. Ionization state of the nebula

Average ionic fractions (weighted by electron density over the nebula) are shown versus $T_5 = T_{\rm eff}/10^5$ K for selected ions in Fig. 2. Concerning neon, Ne^{4+} is the dominant ion over most of the range considered, with an ionization fraction exceeding 50% for $T_5 > 1.2$. Oxygen closely follows neon, but with an overall slightly larger ionization degree. Only O^{2+} and O^{5+} are plotted in Fig. 2. The O^{2+} ion is everywhere residual, with a fractional concentration of only 4×10^{-4} at $T_5 = 1.5$. Carbon is mostly in its highest accessible stage, C^{4+} (not shown), with C^{3+} always small. The ionization grows with $T_{\rm eff}$ due to the rapid increase of the central star's luminosity L (Sect. 4.1.1). The trends just described for D10C1A sequence are relevant to all model sequences considered herein.

5.3. Electron temperature and Balmer line excitation

In Fig. 3 the collisional contributions to the line fluxes of Hα, Hβ, and Hγ are shown relative to the respective Case B recombination fluxes, again for sequence D10C1A. Also shown is the average $T_{\rm e}$ of the nebula in units of 10^5 K. Owing to the high $T_{\rm e}$, the collisional excitation of H I is considerable.

For increasing $T_{\rm eff}$, $T_{\rm e}$ first increases due to the combined effect of the increasing average primary photon energy (proportional to $T_{\rm eff}$) and the decreasing concentration of the important coolant H^0 (Lyα line). Concerning the collisional excitation of the Balmer lines, more sensitive to $T_{\rm e}$ than Lyα itself, this increase of $T_{\rm e}$ is sufficient to overcome the decrease of H^0. However, as $T_{\rm eff}$ further increases, $T_{\rm e}$ decreases due to enhanced cooling by CNO collisional UV lines (Fig. 11). This, together with the decrease of the H^0 concentration, makes the collisional excitation of H I to decrease rapidly.

The shifted curves drawn in Fig. 3 over $T_5 = 1.2$–1.4 correspond to the variant in which the shell covering factor is $f = 0.5$ (Sect. 4.1.2); in these alternative models, the electron density is multiplied by a factor slightly less than $2^{1/2}$ and, due to enhanced H^0 concentration, the collisional excitation is more effective.

Considering the original D10C1A models, but with pre-Nahar (larger) oxygen recombination coefficients (Sect. 4.3.1), the CNO abundances are lowered (Sect. 5.4) and the enhanced $T_{\rm e}$ results in curves (not shown for clarity) that almost exactly overlap those of the $f = 0.5$ variant.

For this set of atomic data (set A, Anderson et al. 2002), the relative collisional excitation of Hα is moderately larger than that of Hβ and the Hα/Hβ ratio will depend only weakly on physical conditions, being always close to the recombination value. Also the relative excitations of Hγ and Hβ are similar and the Hγ/Hβ ratio will be almost independ of physical conditions (except for effects related to departure from Case B; Sect. 5.5).

However, in the case of set F (sequence D10C1F, upper part of Fig. 4), that could legitimately be taken as the "standard choice" until recently, the effective collisional excitation of Hα (Callaway 1994, plus cascades from upper levels) is about as in set A, but excitation of Hβ and, particularly, Hγ (Aggarwal et al. 1991) is much stronger. In contrast, using set G (Giovanardi et al. 1987), collisional excitation is much reduced for Hβ and Hγ but not for Hα (sequence D10C1G, lower part of Fig. 4) and the Hα/Hβ ratio will be enhanced by electron collisions at large $T_{\rm e}$'s.

In conclusion, the Balmer lines can no more be considered as pure recombination lines. Not only will the predicted Balmer decrement depend on assumptions about the collisional rates (Sect. 5.5), but the abundance determinations will depend directly on the collisional excitation of Hβ (Sects. 5.4 and 5.6). A proper analysis of these effects requires a sufficiently large set of models.

5.4. Oxygen and neon abundances

The abundances of oxygen and neon relative to their respective solar values, $(O/H)/(O/H)_\odot$ and $(Ne/H)/(Ne/H)_\odot$, with $(O/H)_\odot = 5 \times 10^{-4}$ (Allende Prieto et al. 2001) and $(Ne/H)_\odot = 1.25 \times 10^{-4}$ (Anders & Grevesse 1989)[2], are plotted in Figs. 5 and 6 respectively.

[2] Since $(Ne/O)_\odot$ is based on solar energetic particles and was not revised (e.g., Asplund et al. 2004), the recent downward revision of $(O/H)_\odot$ should normally be accompanied by a similar downward revision of $(Ne/H)_\odot$. Nonetheless Ne/O is indeed ~0.25 by number in

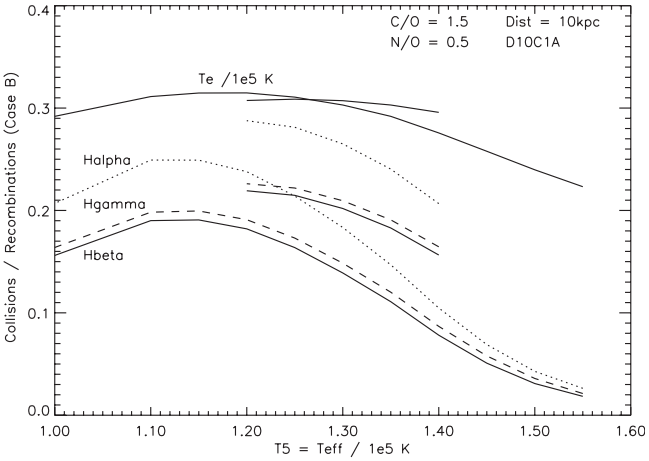

Fig. 3. Nebular electron temperature T_e in units of 10^5 K (upper solid line) and collisional excitation of the Balmer lines Hα (dotted line), Hβ (lower solid line), and Hγ (dashed line) versus $T_5 = T_{\rm eff}/10^5$ K in D10C1A models. (The collisional contribution to each emission line is relative to the corresponding Case B recombination intensity.) Results for the variant with covering factor $f = 0.5$ are shown for $T_5 = 1.2-1.4$.

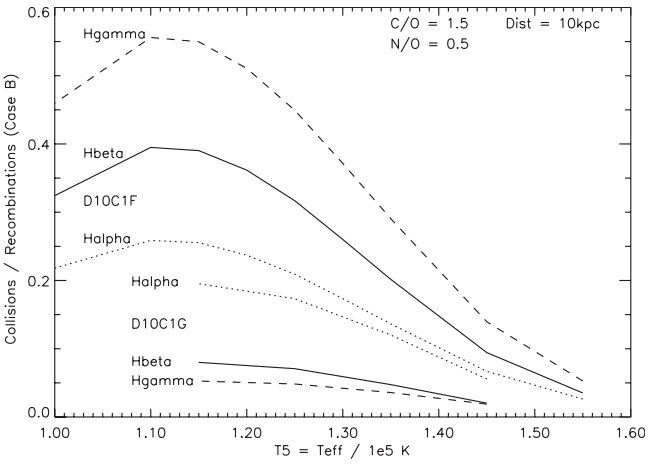

Fig. 4. Same as Fig. 3 for model sequences D10C1F (*upper part*, for $T_5 = 1.00-1.55$) and D10C1G (lower part, for $T_5 = 1.15-1.45$).

A striking aspect is the very steep increase of O/H with $T_{\rm eff}$, an obvious consequence of the small fractional concentration of O^{2+} and the rapid increase of L with $T_{\rm eff}$ (Sect. 4.1.1). For high $T_{\rm eff}$, the very small fractional concentration of O^{2+} (Fig. 2) implies a large O/H to account for the observed [O III]λ 5007 line (at $T_5 = 1.5$, O/H is half solar, with the ionization correction factor, $icf \sim 2500$ in D10C1A). The large CNO abundance will also result in stronger recombination lines (Figs. 10 and 12). For low $T_{\rm eff}$, O/H is very small (typically, 1/100 to 1/400 times solar at $T_5 = 1$), in agreement with the findings of R02 and J02, but a lesser fraction of neon is in the form of Ne^{4+} (Fig. 2) and Ne/H must be large to account for the observed [Ne V] line intensity (typically, Ne/O = 5 to 15 times solar at $T_5 = 1$), again in agreement with J02 results. The abundance of neon increases again moderately for high $T_{\rm eff}$

Galactic PNe (e.g., Kingsburgh & Barlow 1994) and this typical value is preferred herein to the actual solar value of 0.15.

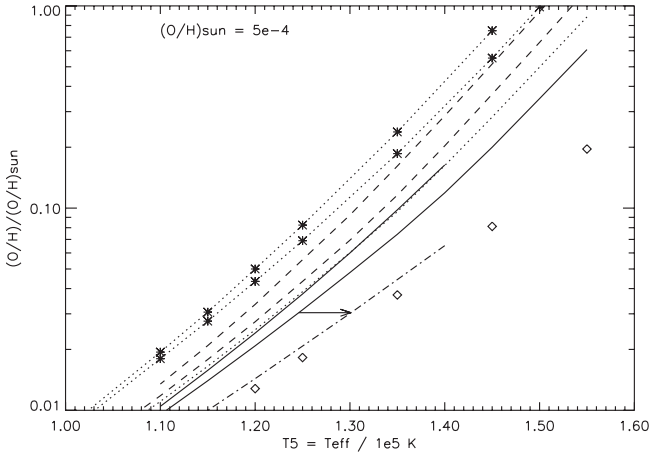

Fig. 5. Oxygen abundance in solar units versus $T_{\rm eff}$ for some model sequences. Dotted line: D10C1A sequence. Lower and upper dotted lines with asterisks: D15C1F and D15C7F. Lower solid line: D10C1AnB, identical to D10C1A, but allowing for departure from case B recombination. Upper solid line: D10C7AnB. Dash-dotted line: variant of D10C1AnB with covering factor $f = 0.5$. Diamonds: variant of D10C1AnB with pre-Nahar oxygen recombination. Lower and upper dashed lines: D15C1AnB and D15C7AnB.

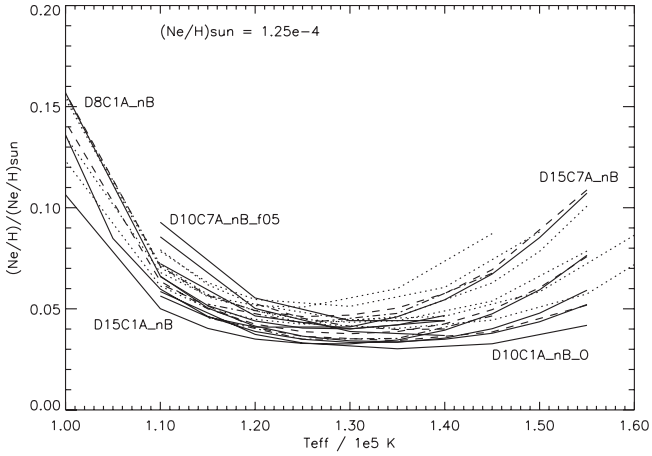

Fig. 6. Neon abundance in solar units versus $T_{\rm eff}$ for all model sequences. Dash-dotted, dashed and dotted lines: Case B model sequences using data sets G, F, and A respectively. Solid lines: non-Case B model sequences using data set A. A few extreme solid lines are labelled: index nB is for "non-Case B"; index O for pre-Nahar oxygen recombination; index f05 for covering factor $f = 0.5$. $(\rm Ne/H)_\odot$: see footnote in Sect. 5.4.

owing to the lowering of the [Ne V] emissivity accompanying the decrease of T_e and the slight decrease of Ne^{4+}/Ne. For intermediate $T_{\rm eff}$'s, Ne/H goes through a shallow minimum, being almost stable at $\sim$1/(25 $\pm$ 4) solar (Fig. 6) and reflecting the constancy of Ne^{4+}/Ne over most of the interval considered. As a consequence, Ne/O *is a strongly decreasing function of* $T_{\rm eff}$ (Sect. 6.3).

The full set of model sequences is included in Fig. 6 to underline the remarkable insensitivity of Ne/H to assumptions at any given $T_{\rm eff}$. On the contrary, the scatter of O/H reaches one order of magnitude and sequences are selected to highlight important features. In Fig. 5, the dotted curves represent

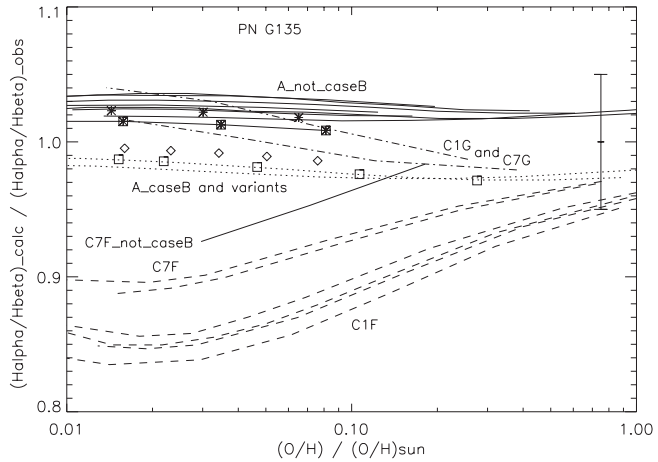

Fig. 7. Computed over observed Hα/Hβ intensity ratio versus O/H in solar units for all model sequences. Dash-dotted, dashed and dotted lines: Case B model sequences using data sets G, F, and A respectively. Solid lines: non-Case B model sequences using data set A. Isolated solid line with larger slope: non-Case B C7F models, as labelled. Symbols near to dotted lines: different (unspecified) variants of Case B D10C1A models. Asterisks and asterisks within squares linked by a solid line: variants of non-Case B model sequence D10C1A and D10C7A respectivelky, assuming a covering factor $f = 0.5$. The observational uncertainty is shown as the vertical bar.

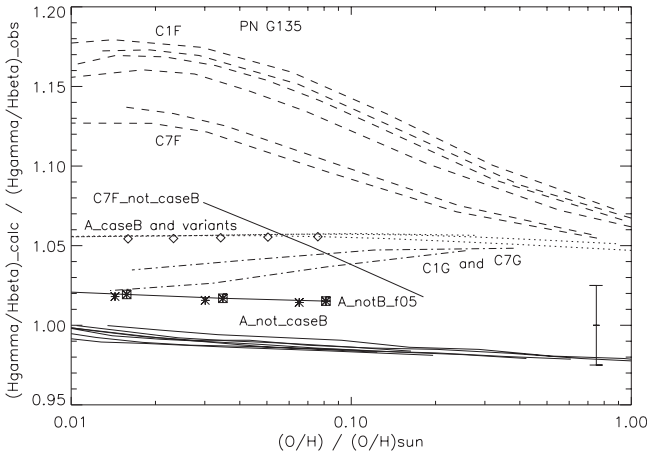

Fig. 8. Same as Fig. 7 for Hγ/Hβ.

Case B results, while all others are non-Case B results. Firstly, O/H is larger at 15 kpc (dashed lines) than at 10 kpc (solid lines) and is larger for larger C/O (smaller T_e). Secondly, using the pre-Nahar recombination coefficients for oxygen leads to lower O/H (diamonds, compared to the lower solid line). The same occurs if the covering factor is reduced to $f = 0.5$ (dash-dotted line, linked to the case $f = 1$ by an horizontal arrow in Fig. 5). Thirdly, under Case B, the larger Hβ emissivity must be compensated by a larger O/H: the Case B D10C1A (upper simple dotted line) almost coincides with the non-Case B D10C7A. Forthly, the Hβ emissivity is the largest when set F is adopted: for illustration, the Case B D15C1F and D15C7F (dotted curves with asterisks) correspond to the highest O/H obtained in the present sample.

These results may give an impression that seemingly "reasonable" changes in atomic physics and/or astrophysical assumptions can change O/H by large factors, thus making the modelling exercise hopeless, and, more particularly, allowing the oxygen abundance to become more or less arbitrarily small for sufficiently small $T_{\rm eff}$. It will be apparent that this is by no means the case, once *other aspects* are taken into account (Sect. 6.1).

The steep, monotonous, variation of O/H as a function of $T_{\rm eff}$ for any model sequence suggests that O/H could be used as main variable instead of $T_{\rm eff}$. In fact, if both $T_{\rm eff}$ and O/H are required because there is no one to one correspondance, particularly when some variants are considered, O/H has the advantage to further correlate with T_e, which helps to outline significant trends. In the next sections, O/H will be most often adopted as the main variable, with [O/H] restricted to the interval $(-2, 0)$.

5.5. Balmer line relative intensities

Predictions for the first three Balmer lines are shown in Fig. 7 (Hα/Hβ) and Fig. 8 (Hγ/Hβ) for all model sequences of Table 2. Using O/H as the main variable, natural groups of sequences, primarily controled by the adopted H I collisional rates (Sects. 4.3.2 and 5.3), become apparent. When collisional excitation rates are far from being proportional to recombination excitation rates (sets G and F), the predicted line ratios depend on conditions, being closer to the recombination values for lower T_e's (large O/H and/or C/O).

The different symbols that are almost superposed on the dotted lines in Fig. 7 correspond to the different variants previously considered for D10C1A. Thus, for set A and adopting the Case B approximation, Hα/Hβ is not only independent of conditions (C/O and variants), but in fair agreement with observation ($\sim -2\%$), whereas Hγ/Hβ, which is observed below its Case B value, is predicted $\sim$5.5% too large. Using set G and Case B, predictions are satisfactory, with Hα/Hβ being now slightly large ($\sim +1.5\%$) and Hγ/Hβ barely too large ($\sim +3\%$). In contrast, Hβ/Hα and, particularly, Hγ/Hβ are predicted systematically much too large in set F models, at least for small or moderate O/H. The impression that C7F models are less discrepant than C1F models is partly misleading, because the larger the value of C/O, the smaller the maximum allowed O/H is (Sect. 6.1.2).

The use of set A and allowing for departure from Case B (solid lines in Figs. 7 and 8) should a priori provide the best physical description of the PN G135 shell. Results for Hγ/Hβ ($\sim -1\%$) are neatly improved relative to Case B, but the agreement for Hα/Hβ is about as before ($\sim +2.5\%$). While predictions for the Balmer decrement are generally insensitive to changes in *astrophysical* assumptions, an exception is the $\sim +3\%$ upward shift of Hγ/Hβ under non-Case B conditions, induced by decreasing the covering factor from unity to $f = 0.5$ (asterisks in squares linked by a solid line for D10C7AnB in Fig. 8). This effect is due to the sensitivity of the Hγ emissivity to the Lyα optical depth in the range of column densities typical of PN G135: Hγ/Hβ is shifted from slightly small to slightly large, suggesting that, with sufficiently accurate observations, inferences about the geometry of the shell could

be possible. The present data are best accounted for assuming $f = 3/4$. Meanwhile, the predicted Hα/Hβ ratio is improved, being brought back to +1.5% of the observed value for D10C7AnB models. For comparison, non-Case B models using data set F (and O/H < 0.04 solar; Sect. 6.1.2) are off by over 7% for both Hα/Hβ and Hγ/Hβ, even in the most favourable conditions (C7, $f = 1$). By analogy, set G meets difficulties at predicting correctly Hα/Hβ in non-Case B situations, whereas it is marginally compatible with observation of Hγ/Hβ if $f \sim 0.5$, that is, if f is given its "minimum" value from the standpoint of departure from Case B (Sect. 4.2).

It is therefore possible to infer from observation that the collisional rates for transitions $1s-5$ obtained by Aggarwal et al. (1991) are too large compared to those for $1s-4$. With the same data, Hα/Hβ is predicted significantly too weak, suggesting again an excess of collisions $1s-4$, but the uncertainty attached to the intensity of Hα may be too large to reach strong conclusions.

Thus, for opposite reasons, *data set G (Giovanardi et al. 1987) and, most particularly, data set F (Aggarwal et al. 1991) are difficult to reconcile with the observed intensities of the first Balmer lines in PN G135*, whereas data set A is acceptable within the uncertainties, when departure from Case B recombination is allowed. *Non-Case B models making use of set A (Anderson et al. 2002) and assuming a covering factor slightly less than unity provide the most satisfactory relative line intensities*.

5.6. Helium abundance

5.6.1. A methodology for helium

Under pure Case B recombination excitation for the Hβ and He II λ 4686 lines and assuming $T_e = (2-3) \times 10^4$ K, He/H by number is only 0.075–0.079, despite the +5.8% correction of the intensity ratio (Sect. 3.2.2). The He/H determination is lowered by departure from Case B for the Hβ emissivity (Sect. 5.5), but enhanced by the collisional excitation of Hβ (Sect. 5.3).

As shown in Fig. 9, the He/H values indicated by the different photoionization models (*all* precisely fulfilling *all* basic observational requirements) encompass a broad range (0.066–0.116), due to (1) the various atomic data sets used; (2) the various assumptions concerning the H I line radiative transfer (Case B or not); (3) the range of T_e obtained in different models, depending on T_{eff}, C/O, and other assumptions.

Here, instead of determining ab initio an illusory He/H from models, we try to gain insight into both the collisional excitation of the Balmer lines and the astrophysical parameters of PN G135, taking advantage of: (1) the absence of He I; (2) the good accuracy of the He IIλ 4686 intensity; (3) the high accuracy of the atomic data relevant to He II (hydrogenic recombination at low electron density, negligible collisional excitation); (4) the small departure from Case B recombination for He IIλ 4686 (taken into account in practice); and (5) the a priori narrow range of He/H allowed by common astrophysical wisdom.

As a matter of fact, it is extremely unlikely that He/H in PN G135 could be less than the pre-Galactic value $(He/H)_P$.

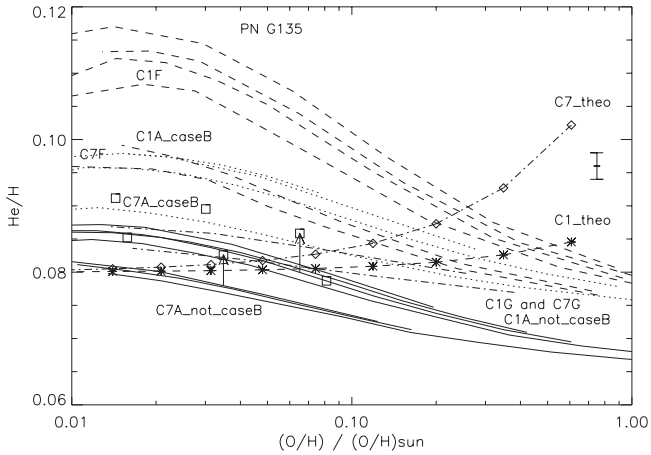

Fig. 9. Helium abundance by number relative to H versus O/H in solar units for all model sequences. Dash-dotted, dashed and dotted lines: Case B model sequences using data sets G, F, and A respectively. Solid lines: non-Case B model sequences using data set A. Non-Case B models obtained using set A and a covering factor $f = 0.5$: squares (upper squares: C1 models; lower squares: C7 models), linked to their respective $f = 1$ model sequences by vertical arrows. Vertical bar: observational uncertainty (±2.5%). Asterisks (linked by a dashed line) and diamonds (linked by a dash-dotted line): theoretical guesses corresponding to C1 and C7 models respectively (Sect. 5.6.1).

Helium depletion by gravitational settling (e.g., Edelmann et al. 2003), is excluded in the atmosphere of giant stars with deep convective envelopes, undergoing mass loss. Recent estimates for $(He/H)_P$ range from 0.0811 (Izotov et al. 1999) to the most elaborate 0.0786 (Luridiana et al. 2003). At the birthplace of the parent star of PN G135, the ISM was either deprived of metals or modestly enriched by Pop III massive star explosions, whose chemical yields favour the production of O and Fe rather than that of He (e.g., Woosley & Weaver 1995). In both cases, He/H was probably close to 0.080. It can also be noted that He/H is about 0.082 in K 648. Assuming tentatively a ratio of incremental enrichment by number $\Delta He/\Delta C \sim 10$, typical of third dredge-up in low-mass stars (e.g., Marigo 2001), a first approximation to the value of He/H expected in PN G135 is:

$$He/H = 0.080 + 10 \times (C/H),$$

where the pre-stellar carbon content of the PN has been neglected and any endogenous or exogenous helium possibly associated with the production of nitrogen and pre-stellar oxygen is assumed to be incorporated into the adopted initial He/H. This "theoretical" expression for He/H is overplotted in Fig. 9 in both cases under study.

5.6.2. Assumptions versus O/H determination

Figure 9 presents analogies with Figs. 7 and 8, but contains new information, as the model helium abundance reflects the *absolute* collisional excitation rate of Hβ rather than relative rates.

Considering first the Case B approximation, the old data set G (small collisionnal rates) leads to He/H close to expectation for "moderate" O/H: the C1G and C7G curves cut the

theoretical curves at O/H = 1/7 and 1/23 solar, respectively. In the case of the most recent data set, O/H ∼ 1/3.6 and 1/11 solar for the C1A and C7A curves, respectively. Finally, O/H ∼ 1/2 and 1/8 solar for the C1F and C7F curves. The split between the C1 and C7 results, reflecting the differences in T_e, is large and systematic. On the other hand, D does not significanttly bear on the He/H determination.

Considering instead the a priori most relevant combination of physical assumptions, namely, set A with departure from Case B (solid lines), the predicted He/H is lowered, with O/H ∼ 1/16 and 1/66 solar for C1AnB and C7AnB, respectively. Nonetheless, this combination does not imply that only very small O/H's would be allowed. First, the curves are almost flat for small O/H and the uncertainties broaden the range of accessible O/H's. Moreover, as for the Balmer lines, non-Case B results are sensitive to the covering factor. For variants of D10C1AnB and D10C7AnB models obtained with $f = 0.5$ (squares in Fig. 9), the theoretical curves are crossed at O/H = 1/7.5 and 1/22 solar for C1 and C7 respectively. Adopting again $f = 3/4$, then O/H ∼ 1/10 (C1) and 1/40 (C7) solar. A plausible picture seems to emerge since, (1) such oxygen abundances will prove to be in agreement with other criteria (Sect. 6.1); (2) the asymmetry of the PN suggests that f could be somewhat less than unity (Sect. 4.1.2); and (3) the computed Balmer decrement is most satisfactory in these same conditions (Sect. 5.5).

Inspection of Fig. 9 makes it clear that many models should be discarded because they imply too much helium in the shell, particularly those obtained assuming Case B. The non-Case B C7F sequence (not shown) is slightly above the non-Case B C1A sequences (upper solid lines) and cuts the theoretical curve at O/H ∼ 1/17 solar. Thus, in this diagram, Aggarwal et al. (1991) data can be made consistent with observation only if $f = 1$ and C/O is very large, which will however probably *not* be the case (Sect. 7). Conversely, since Case B models based on set G lead to relatively small helium abundances and since some departure from Case B is likely, the suggestion is that *the collision strengths provided by Giovanardi et al. (1987) for transitions* 1−4 *of hydrogen are too small*.

5.6.3. On the determination of He/H

As increasingly realistic data and assumptions are introduced − Anderson collision strengths, departure from Case B, moderate O/H (see later), covering factor somewhat less than unity, He II stellar absorption lines, etc. −, the vast range of initialy accessible He/H (Fig. 9) boils down to a much narrower range, which includes in a natural way the He/H value that would be expected on quite general, indisputable grounds. Thus, the photoionization model analysis does imply an helium abundance close to 0.081 and this determination is the result of a fairly subtle balance between relatively large, antagonistic effects.

Then, it is perhaps not surprising if significantly different He/H were obtained by previous authors. The present analysis can help us to gain insight into the nature of previous calculations. Using the code PHOTO in conditions met in the present sample ($T_5 = 1.25$, $L = 10^{37}\,\mathrm{erg\,s^{-1}}$), R02 obtained He II$\lambda$ 4686 = 75 (usual units) for He/H = 0.08. The observed intensity of 82 (Hβ corrected from He II only) then leads to He/H = 0.0875, consistent, for very small O/H and moderate C/O, with a weak, Giovanardi-like, collisional excitation of Hβ under Case B (upper dash-dotted line in Fig. 9): both the atomic data and the physical treatment used are inadequate to reach quantitative conclusions in the conditions prevailing in PN G135.

On the other hand, J02 obtained, but did not comment on, the astonishingly low value He/H = 0.066. In the event that their computation was performed under strict Case A, the He/H counterpart under Case B would be He/H ∼ 0.105, reminiscent of Aggarwal-like collisional strengths for vanishingly small O/H (dashed lines in Fig. 9). However, it is much more likely that Anderson's collision strengths were effectively implemented in CLOUDY, the code used by J02, and that, due to the "extremely" low T_e (consequence of their C/O = 23 and N/O = 52) in the model they put forth, the collisional excitation of Hβ was considerably reduced. Indeed, in the present grid of results, the standard non-Case B models with Anderson's data tend asymptotically to He/H = 0.066 for large O/H, that is, for low T_e (solid lines in Fig. 9). This remarkable agreement with the He/H found by J02 suggests that their computations were done with a treatment for departure from Case B leading to essentially the same result as NEBU (Interestingly, CLOUDY and NEBU outputs had so far not been compared in such physical conditions; see Péquignot et al. 2001). And the oddness of the resulting He/H indicates that the astrophysical assumptions adopted by J02 were probably wrong. In their attempt to increase O/H as much as possible (at low $T_{\rm eff}$), J02 implicitly sacrificed the helium abundance.

Thus, the present computations allowed us to (1) understand the different results; (2) check the *numerical* agreement of the different codes in comparable conditions; and (3) point out some weaknesses in previous attempts to model PN G135. The physically most realistic description of the PN is consistent with He/H = 0.080−0.082. Given the freedom left by the value of f and the observational uncertainties, the oxygen abundance is not yet strongly constrained: in the best descriptions, *a value not exceeding about one tenth solar is indicated for O/H*. We now turn to other spectroscopic constraints.

5.7. Undetected emission lines

Predicted line intensities (units $I_{\mathrm{H}\beta} = 100$) versus $T_5 = T_{\rm eff}/10^5$ K are shown in Fig. 10 for optical collisional and recombination lines of D10C1A models.

The theoretical intensities of C IV λ 7726 and O IV λ 7713 are typically 40 percent of their optical counterparts. Importantly, *if* these far-red lines were *really not detected*, even with an upper limit one order of magnitude better than in the optical (Sect. 3.2), then the upper limits set on the C^{4+} and O^{4+} abundances should be *four times more stringent* than those implied by the leading optical lines shown in Fig. 10 (see also Fig. 15).

As $T_{\rm eff}$ (and L) increases, the rapid decrease of the predicted [Ne IV] and [Ne III] intensities is due to the combined

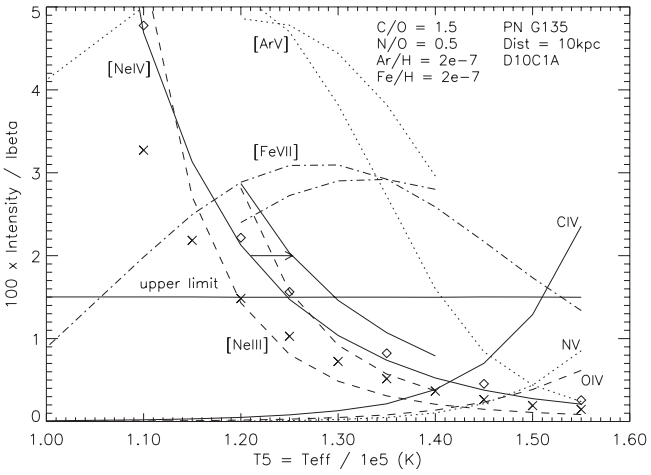

Fig. 10. Predicted intensities in units $I_{H\beta} = 100$ versus $T_{\rm eff}$ for optical lines in model sequence D10C1A and some variants. The forbidden lines are [Ne III] 3869+3968, [Ne IV] 4714+25, [Ar V] 7005+6435 and [Fe VII] 6087 and the permitted lines are C IV 4658, O IV 4632 and N V 4945. Curves for [Ar V] and [Fe VII] correspond to fixed abundances. Horizontal line $I = 1.5$: upper limit 1−1.5 adopted for these lines. Shifted curves drawn from $T_5 = 1.2$−1.4: variant of D10C1A in which $f = 0.5$; an horizontal arrow indicates the shift for [Ne IV]. Diamonds and crosses: [Ne IV] intensity for variants in which either O^{2+}–O^{4+} or Ne^{3+} have modified recombination coefficients (Sect. 4.3.1).

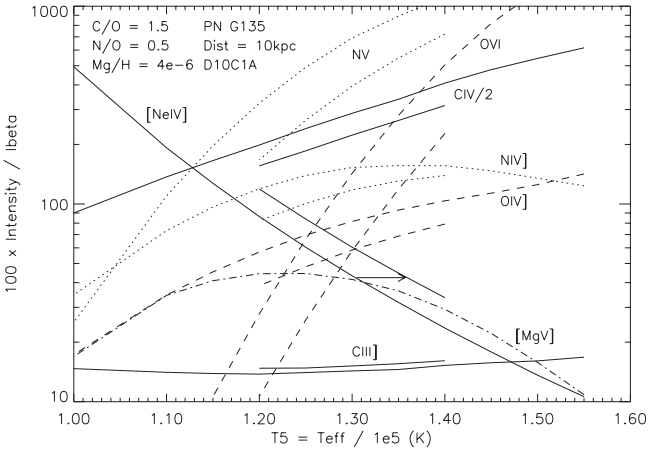

Fig. 11. Predicted intensities in units $I_{H\beta} = 100$ versus $T_{\rm eff}$ for the UV lines in model sequence D10C1A. Lines are C III] 1908, C IV 1549 (intensity divided by 2 in the display), N IV] 1487, N V 1240, [O IV] 1400, O VI 1034, [Ne IV] 2423 and [Mg V] 2782. The curve for [Mg V] corresponds to a fixed Mg/H. Shifted curves and arrow for $T_5 = 1.2$−1.4 as in Fig. 10.

effect of the decrease of Ne/H (Fig. 6) and the decrease of the fractional concentration of the corresponding ions (Fig. 2). For high $T_{\rm eff}$, these lines are further quenched by the lowering of $T_{\rm e}$ (Fig. 3). While [Ne III]λ 3869, singled out in previous works (Sect. 3.1), imposes an important lower limit ($T_5 > 1.20$), multiplet [Ne IV]$\lambda\lambda$ 4714+25 turns out to impose an even more stringent one ($T_5 > 1.25$), for which the predicted [Ne III] intensity is still consistent with the value measured by R02. *This general feature of the PN G135 models will confer a fundamental role to [*Ne IV*], also favoured by its lesser sensitivity to possible inaccuracies of the atomic data.*

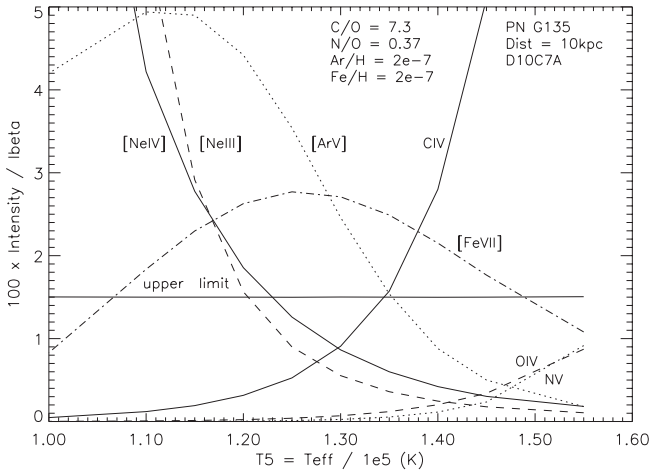

Fig. 12. Same as Fig. 10 for model sequence D10C7A.

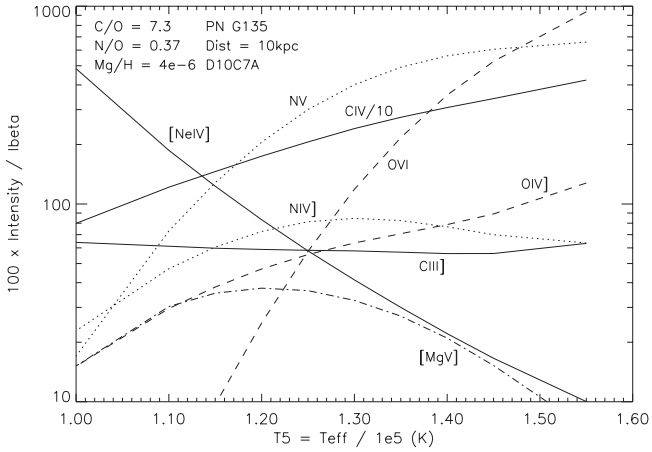

Fig. 13. Same as Fig. 11 for model sequence D10C7A; the intensity of C IVλ 1549 is divided by 10 for display.

Predictions for UV lines are shown in Fig. 11. The strongest lines are [Ne IV] and O VI for low and high $T_{\rm eff}$'s respectively. For the assumed (C/O, N/O), C IV and N V have intensities of the same order and dominate over most of the $T_{\rm eff}$ range shown. The intensity of C III] is weak and almost constant.

In both Figs. 10 and 11, collisionally excited line intensities are also drawn over the interval $T_5 = 1.2$−1.4 for the variant in which $f = 0.5$.

Other aspects of multiplet [Ne IV] are as follows. In Fig. 10, the diamonds are obtained when the pre-Nahar oxygen recombination coefficients are used: the effect in this case is negligible. Taking into account departure from Case B (not shown) has a similarly negligible effect. Finally, the crosses obtain when the Ne^{3+} recombination coefficient is divided by a factor 1.5 (Sect. 4.3.1): the [Ne IV] intensity is then divided by a factor ∼1.43.

Predicted line intensities for sequence D10C7A are shown in Figs. 12 and 13. Compared to D10C1A, the larger C/O ratio results in stronger carbon lines (similarly, the nitrogen lines are slightly weaker). Other line intensities are almost unaffected, except for a tendency of the UV lines N V and O VI to level off at the highest $T_{\rm eff}$'s. At low $T_{\rm eff}$, gas cooling is mainly due to

hydrogen and all line intensities are simply proportional to the relevant elemental abundances.

6. Discussion

6.1. Range of acceptable O/H

6.1.1. [Ne IV] and lower limit to O/H

The interplay of different parameters must be taken into account. Consider the lower limit to O/H corresponding to the lower limit to $T_{\rm eff}$ imposed by [Ne IV]. In Fig. 5, the horizontal arrow indicates that O/H is significantly decreased in the variant $f = 0.5$, compared to the $f = 1$ case, suggesting that an arbitrarily small O/H lower limit can be obtained just by assuming a small covering (or filling) factor. However, the horizontal arrow in Fig. 10 indicates that the lower limit to $T_{\rm eff}$ must then be increased, resulting in an effective minimum to O/H which is only slightly less than in the $f = 1$ case. In addition, arbitrarily small f's are not allowed because the $T_{\rm eff}$ lower limit would grow further until no acceptable solution is left. Consideration of timescales (Sect. 6.4) will independently show that very large $T_{\rm eff}$'s are probably inapropriate. In this example, the minimum f may not be much smaller than 0.5. The same remarks can be made for models involving changes in the primary continuum shape (Sect. 6.5).

These comments are illustrated in Fig. 14, in which the predicted intensity of multiplet [Ne IV] is plotted versus O/H for all available models. Remarkably, except for a few variants considered below, each category of model sequence curves (usual notations) displays a very small scatter (± 5−7%). At a given O/H, the largest [Ne IV] intensities correspond to data set F (dashed lines), followed by data sets G and A (almost undistinguishable, dotted lines) and then, barely separated, data set A with departure from Case B (solid lines). The latter case, that corresponds to the preferable physical description and to the most conservative conclusion, provides O/H lower limits that range from 3.2% to 3.8% solar, according to the (here unspecified) details of the astrophysical assumptions. Thus:

$$({\rm O/H})/({\rm O/H})_\odot > 0.035 \pm 0.003,$$

or, simply taking the lower envelope:

$$[{\rm O/H}]_{\rm min} = -1.5.$$

Models with covering factor $f = 0.5$ (asterisks in Fig. 14) are just slightly shifted from their standard counterparts (solid lines), indicating that the geometry of the shell is of little concern in this case. In these conditions, a more precise limit is $[{\rm O/H}] > -1.52$.

Coincidentally, the shifts corresponding to unrelated variants, namely those obtained with (1) the pre-Nahar oxygen recombination coefficients and (2) the Ne^{3+} recombination coefficient divided by 1.5, lead to similar downward [Ne IV] intensity shifts: the squares linked by a dotted line and the crosses are all shifted from D10C1A models. About the same shift also applies to any other sequence, as shown by the squares linked by dashed lines (pre-Nahar variant of D10C1F) and solid lines (pre-Nahar D10C1AnB). Concerning the primary continuum, using realistic model atmospheres leads to a significant *upward* shift of $[{\rm O/H}]_{\rm min}$ (Sect. 6.5).

Thus the only factors that may conceivably decrease the O/H lower limit deal with the recombination coefficient of Ne^{3+}, for which only conjectures can be made, and those of O^{2+} and O^{3+}, for which there is every reason to believe that Nahar's data should be preferred to earlier estimates. The comparison between results for N^+ obtained by Nahar & Pradhan (1997) and Kisielius & Storey (2002) suggests that the uncertainty attached to the data of Nahar (1999) does not exceed 15%. Summing up reasonable uncertainties in the different recombination coefficients, the non-Case B pre-Nahar curve (solid line linking squares in Fig. 14) can be considered as a conservative lower envelope of the [Ne IV] curves.

In conclusion, the [Ne IV] intensity correlates tightly with O/H in a large sample of models in which all conceivable astrophysical and atomic physics parameters of relevance are varied. *A very conservative lower limit to the oxygen abundance of PN G135 is 2% of the current solar value*. However, accepting standard recombination coefficients for Ne^{3+}, O^{2+}, and O^{3+}, particularly those obtained by Nahar (1999) for oxygen, a more likely lower limit is 3.1% solar. *This lower limit* $[{\rm O/H}]_{\rm min} = -1.5$ *is large enough to clearly exclude the interval* $-2.9 < [{\rm O/H}] < -2.2$ *obtained by R02 from models*. Reasons that can qualitatively explain this discrepancy were exposed in Sect. 3.1 (see also Sect. 6.1.3). Also, part of the gap between the present and R02 model results is probably due to the use of pre-Nahar data by R02 (and J02).

6.1.2. C IV and upper limit to O/H?

Constraints imposed by the O IV and O V intensities are interesting in that they are independent of any complementary assumption, but they are relatively weak. For model sequence D10C1A (Fig. 10) an upper limit $T_5 < 1.60$ (or, from far-red lines, <1.53) is obtained. Nonetheless, even for this rather moderate C/O, the C IV upper limits result in $T_5 < 1.50$ (C IVλ 4658) or $T_5 < 1.40$ (C IVλ 7726). Considering D10C7A (Fig. 12), the upper limit to $T_{\rm eff}$ imposed by C IV (optical and far-red lines) is now just slightly more than $T_5 = 1.30$, approaching the lower limit of 1.22 dictated by [Ne IV]. Provided that C/O > 1/3, the C IV lines are probably the strongest recombination lines, unless N/C is exceedingly large in PN G135.

In Fig. 15 the predicted intensity of C IV versus O/H is shown. The curves clearly split in accordance with the values adopted for C/O. Nonetheless, a scatter of the C IV intensity ∼±15% at a given O/H is apparent. The solid horizontal line indicates the upper limit to the C IVλ 4658 intensity. The dashed line is again an upper limit to C IVλ 4658, but derived from C IVλ 7726 (Sect. 3.2).

According to current knowledge, C/O is likely to be large in a PN arising from a low-mass low-metallicity star. This is confirmed observationally, e.g., in the case of K 648, where C/O = 7.3. Also C/O is typically 2−5 by number in the atmosphere of low-mass H-deficient stars of the WC and PG 1159 types (e.g., Koesterke & Hamann 1997). Carbon could be further selectively enhanced in Pop III stars (Sect. 2.2.2). Considering

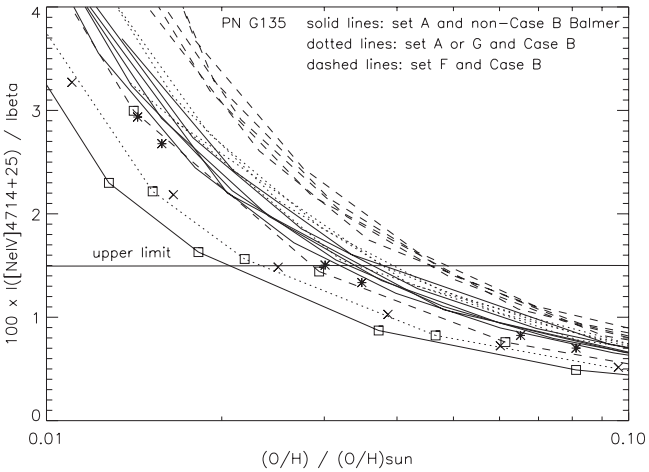

Fig. 14. Predicted intensity of multiplet [Ne IV]λ 4714+25 versus O/H in solar units for all model sequences. Dashed and dotted lines: Case B model sequences using data sets F and G or A respectively. Solid lines: non-Case B model sequences using data set A. Asterisks: variants of non-Case B D10C1A and D10C7A models with covering factor $f = 0.5$. Squares, linked by dashed, dotted, or solid lines (as above): variants with pre-Nahar oxygen recombination coefficients. Multiplication crosses: variants of D10C1A with modified Ne^{3+} recombination.

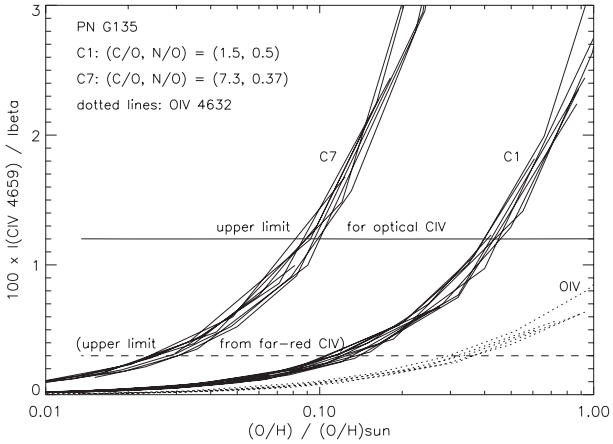

Fig. 15. Predicted intensity of C IVλ 4658 versus O/H in solar units for all model sequences. Solid horizontal line: upper limit to the C IVλ 4658 intensity. Dashed horizontal line: upper limit to C IVλ 4658, as derived from C IVλ 7726. Intensity of O IVλ 4632 shown for comparison.

C7 models, the upper limit to O/H from C IVλ 4658 is (without specifying details of the assumptions):

$$(O/H)/(O/H)_\odot < 0.09 \pm 0.01,$$
$$[O/H]^{opt}_{max}(C7) = -1.$$

The (more tentative) upper limit from C IVλ 7726 is only:

$$(O/H)/(O/H)_\odot < 0.027 \pm 0.002,$$
$$[O/H]^{red}_{max}(C7) = -1.6,$$

that is, about the lower limit obtained in Sect. 6.1.1. Solutions to this potential difficulty can be sought in several directions. Firstly, [O/H] may indeed be close to $[O/H]_{min}$. Secondly, the stringent upper limit adopted by analogy with other far-red

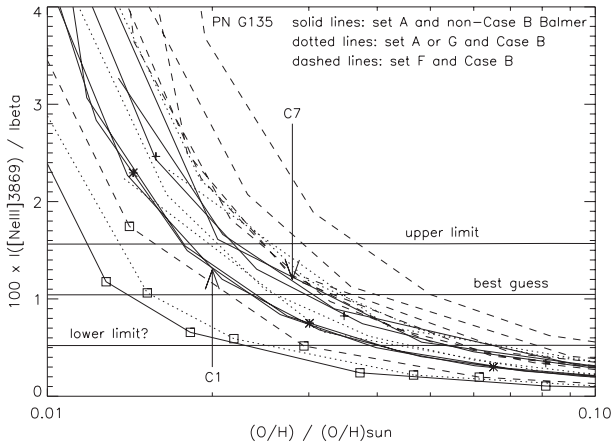

Fig. 16. Same as Fig. 14 for [Ne III]λ 3869. Three solid horizontal lines: best estimated intensity and ± 1-σ error. The question mark attached to the lower limit is to remind that this limit should be taken with caution (Sect. 3.1).

lines (R02) may not apply precisely to the C IVλ 7726 line. Thirdly, C IVλ 7726 may in fact be present in the WHT spectrum, but not explicitly recorded by R02. Finally, C/O may after all be smaller in PN G135 than in the extreme case of K 648: results obtained assuming C/O = 1.5 lead to the more "comfortable" upper limits $[O/H]_{max} = -0.4$ and -0.9, based on the non-detection of λ 4658 and λ 7726 respectively (Fig. 15). Giving reasonable weight to the λ 7726 upper limit and assuming that C/O could hardly be less than 1.5 in PN G135, *it is probably fair to adopt* $[O/H]_{max} = -0.9$. On the other hand, *it is safe to conclude that C/O must be less than 10 by number in PN G135*.

These results demonstrate the interest of deep, high signal-to-noise, far-red spectra of PN G135. Detecting UV lines (Figs. 11 and 13) would obviously be of interest too.

6.1.3. [Ne III] and possible guess for O/H?

The predicted intensity of [Ne III] versus O/H shows a large scatter (Fig. 16), reflecting the strong dependence of this low-ionization line on assumptions. This scatter would be even larger if variations of atomic data directly relevant to the ionization of Ne^{2+} were included.

Considering the non-Case B C7 models, the predicted [Ne III]λ 3869 intensities (upper blend of solid lines in Fig. 16) meet the best observed value for $(O/H)/(O/H)_\odot = 0.03$. Given that these models correspond a priori to the best physical description and to likely astrophysical assumptions, and that, in these conditions, this value of O/H is *also* (1) the lower limit set by [Ne IV]; (2) the most stringent upper limit set by the far-red C IV line; and (3) a good choice from the standpoint of both the Balmer decrement and the He/H ratio, it could be tempting to conclude that the oxygen abundance in PN G135 is indeed:

$$(O/H)/(O/H)_\odot \sim 0.03,$$

then establishing this object as the most oxygen-poor PN known, by a factor of 2.5.

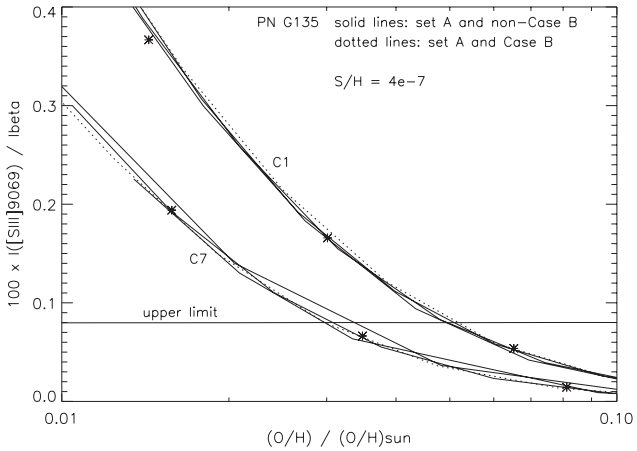

Fig. 17. Same as Fig. 14 for [S III]λ 9069, at fixed S/H.

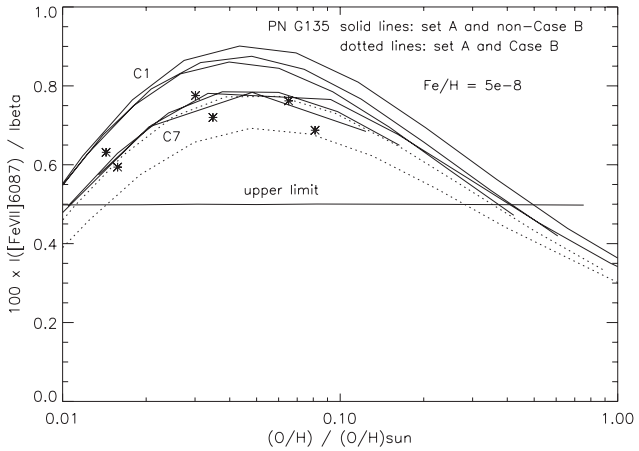

Fig. 19. Same as Fig. 14 for [Fe VII]λ 6087, at fixed Fe/H.

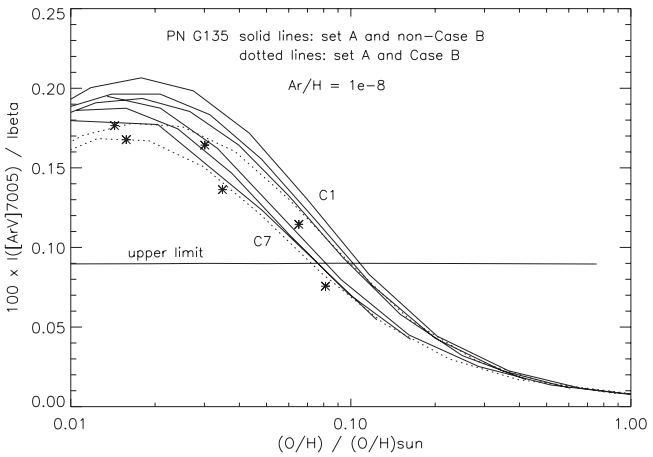

Fig. 18. Same as Fig. 14 for [Ar V]λ 7005, at fixed Ar/H.

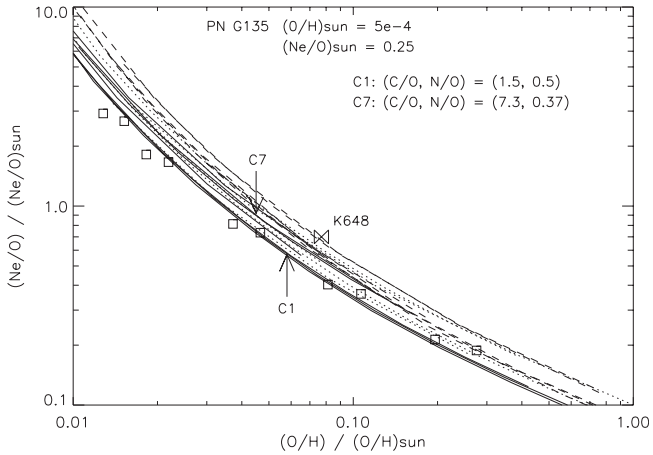

Fig. 20. (Ne/O)/(Ne/O)$_\odot$ versus (O/H)/(O/H)$_\odot$ for all model sequences of PN G135. The butterfly symbol corresponds to our unpublished model for K 648. Lines and other symbols as in Fig. 14. The lower and upper blends of solid lines indicated by arrows correspond to non-Case B C1 and C7 model sequences respectively. (Ne/O)$_\odot$: see footnote in Sect. 5.4.

Unfortunately, this suggestive convergence, which would not hold for, e.g., C1 models, is partly a chance coincidence since a precise solution cannot be firmly documented on the basis of one doubtful intensity and a few upper limits. In the event that the [Ne III] intensity would be exactly confirmed, the factor 2−3 uncertainty affecting the ionization fraction of Ne^{2+} in the extreme conditions of PN G135 (variant model sequences not shown in Fig. 16) would only allow us to set the limits:

$0.01 < (O/H)/(O/H)_\odot < 0.1.$

6.2. Metallicity

Concerning elements heavier than neon, upper limits can be derived using Figs. 17–19. For $(O/H)/(O/H)_\odot = 0.04 - 0.08$, we find $S/H < 4 \times 10^{-7}$, $Ar/H < 8 \times 10^{-9}$ and $Fe/H < 3 \times 10^{-8}$ from [S III]λ 9069, [Ar V]λ 7005 and [Fe VII]λ 6087 respectively. Considering the very large ionization correction factor for [S III] and the large uncertainties affecting the ionization equilibrium of sulfur, the upper limit to S/H is at best indicative and not particularly stringent. On the other hand, since Fe^{6+} and Ar^{4+} are abundant ions of Fe and Ar respectively (Fig. 2), the predicted line intensities are less sensitive to possible errors in the ionization balance. At face value, the limit on [Fe VII] reads [Fe/H] < -3.0, but part of the iron may be locked into dust grains, as in most other PNe. Argon is not depleted into dust and the above limit reads [Ar/H] < -2.3 (Asplund et al. 2004). Given that the α-elements in halo stars with [Fe/H] < -1 tend to be enhanced by $\geq$0.2 dex with respect to iron (e.g., Cayrel et al. 2004), the upper limit to the metallicity of PN G135 is:

[Fe/H] < -2.5.

This upper limit now pertains to the iron abundance in the progenitor star, not the gaseous iron abundance as above. Using the same rule, far-red spectra secured by Barker (1980) for K 648 indicate an Ar/H in harmony with the [Fe/H] of M 15 within (large) uncertainties. *PN G135 may well be a more extreme Pop II object than K 648.*

6.3. Ne/O in PN G135

The stability of Ne/H together with the steep rise of O/H with $T_{\rm eff}$ (Sect. 5.4) can provide a first clue to the likeliest O/H. The plot of Fig. 20 illustrates the strong and highly correlated dependence of Ne/O on O/H. If Ne/O is in PN G135 as in most

PNe, then $(O/H)/(O/H)_\odot = 0.034$ and 0.042 for C1 and C7 models respectively: since this nearly corresponds to $[O/H]_{min}$, a first conclusion is that *Ne/O cannot be significantly larger than solar in PN G135*.

On the other hand, Howard et al. (1997) suspect that, within their estimated error of 0.25 dex, Ne/O may be on average 0.3 dex less than solar in GHPNe. If Ne/O is taken as half solar, then $(O/H)/(O/H)_\odot = 0.068$ and 0.084 for C1 and C7 models respectively. In the relatively well defined example of K 648, Ne/O = 0.17 and C/O = 7.3 (butterfly symbol in Fig. 20). Adopting these ratios for PN G135, a non-Case B model leads to $(O/H)/(O/H)_\odot = 0.060$, compared to 0.077 in K 648. This small difference suggests that, with minor adjustments, *the full set of abundances determined for K 648 could apply to PN G135 as well*, as illustrated by Model M 1 (Tables 3 and 4, Sect. 7). More generally, allowing for Ne/O down to one third solar, values of O/H found in other GHPNe could be obtained.

One aspect of the Ne/O ratio in GHPNe is its large scatter, which seems to be at least partly real. Thus, Ne/O does provide a useful indication, but no secure conclusion can be drawn concerning O/H in PN G135 solely on this basis: a small Ne/O could lead to a large O/H. Nonetheless, O/H cannot be large unless C/O is sufficiently small *as well* (Sect. 6.1.2).

6.4. Timescales, distance and $T_{\rm eff}$

A kinematic timescale for PN G135 is:

$$t_{\rm kin} = 8.0\times10^3 \text{ yrs } \times (r''/5) \times (v_{\rm exp}/30)^{-1} \times (D/10\,\text{kpc}),$$

with r'' the angular radius in arcsec (J02, R02; Sect. 4.1.2) and $v_{\rm exp}$ the current expansion velocity in km s^{-1} (Richer et al. 2003). In this low-Z PN, the AGB wind terminal velocity was probably very low (Habing et al. 1994) and, after having been accelerated, the nebula was probably not slowed down in the Galactic halo (Hippelein & Weinberger 1990). Then assuming, e.g., a linear increase of the expansion velocity with time, the expansion time $t_{\rm exp}$ is twice $t_{\rm kin}$. Adopting the expression:

$$t_{\rm kin}(D) = 8\times10^3 \text{ yrs } \times (D/10\,\text{kpc})$$

and keeping in mind uncertainties in both the derived $t_{\rm kin}$ (±30%, considering the different "$v_{\rm exp}$" and "sizes" available) and the conversion of $t_{\rm kin}$ into $t_{\rm exp}$, it is probably safe to assume that:

$$t_{\rm exp}(D,\zeta) = \zeta \times t_{\rm kin}, \quad 1 < \zeta < 3.$$

Assuming an evolution of the nucleus of PN G135 according to the post-AGB tracks obtained by Bloecker (1995), we use the curves $T_{\rm eff}(t_{\rm evol})$, with $T_{\rm eff}$ taken along the (high-luminosity) pre-turnoff branch, and $Q_{13.6}(t_{\rm evol})$ (number of photons emitted per second above 13.6 eV), parameterized by the mass $M_{\rm nucl}$ of the nucleus, as provided in Fig. 2 of Tovmassian et al. (2001). For the high $T_{\rm eff}$'s considered here, most of the luminosity is emitted above 13.6 eV and $Q_{13.6}$ can be safely converted into a luminosity L, assuming a black body stellar continuum at temperature $T_{\rm eff}$. There are therefore two functions $t_{\rm evol}(M_{\rm nucl}, T_{\rm eff})$ and $L(M_{\rm nucl}, T_{\rm eff})$, with the latter equivalent to a function $T_{\rm eff}(M_{\rm nucl}, D)$, or $M_{\rm nucl}(T_{\rm eff}, D)$, given the relation $L(T_{\rm eff}, D)$ based on the identification of the observed optical flux to the black body flux (Sect. 4.1.1). In Fig. 21, $T_{\rm eff}(M_{\rm nucl})$ is plotted for the 3 values of D considered in our models. A limit is obtained if $T_{\rm eff}$ is given its maximum value $T_{\rm eff}^{\rm max}(M_{\rm nucl})$: this limit nearly coincides with the curve obtained for $D = 6.5$ kpc, which is therefore the smallest conceivable distance $D = D_{\rm min}^{\rm BB}$ to PN G135 in this description (see, however, Sect. 6.5).

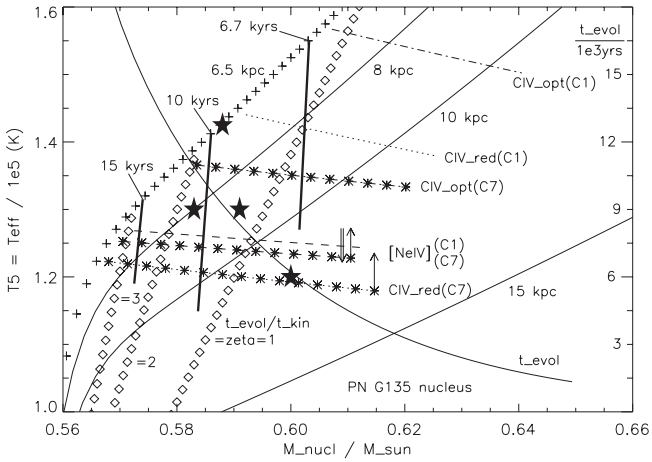

Fig. 21. Solid lines: effective temperature $T_{\rm eff}$ of the nucleus of PN G135, assumed to radiate like a black body, versus nucleus mass $M_{\rm nucl}$ in solar units for distances D = 8, 10 and 15 kpc, as labelled. Cross line: $T_{\rm eff}^{\rm max}(M_{\rm nucl})$, also corresponding to $D_{\rm min}^{\rm BB} = 6.5$ kpc. Solid line labelled "$t_{\rm evol}$": evolution timescale $t_{\rm evol}$ of the nucleus, read on the *right scale* in units of 10^3 yrs. Three steep diamond lines: $T_{\rm eff}$ for $t_{\rm evol}$ equal to 1, 2, and 3 times $t_{\rm kin}$, as labelled, with $t_{\rm kin}$ the kinematic timescale of the PN. Three almost vertical thick solid lines: $T_{\rm eff}$ for $t_{\rm evol}/10^3$ yrs = 6.7, 10, and 15, as labelled. Six almost horizontal lines: limits on $T_{\rm eff}$ due to upper limits on 3 emission line fluxes, as labelled, for non-Case B model sequences computed with H I collision strengths of set A and assuming either C/O = 1.5 (curves labelled C1) or C/O = 7.3 (curves labelled C7, emphasized by asterisks); two dashed lines: lower limit due to multiplet [Ne IV]$\lambda\lambda$4714+25; two dash-dotted lines: upper limit due to C IVλ4658 (labelled C IV$_{\rm opt}$); two dotted lines: upper limit due to C IVλ7726 (labelled C IV$_{\rm red}$). Two upward arrows: effect of assuming a shell covering factor $f = 0.5$ ([Ne IV] and C IV$_{\rm red}$ in C7 sequences). Downward double arrow: effect of dividing the recombination coefficient of Ne^{3+} by a factor 1.5 ([Ne IV] in C7 sequences). Stars: the 4 models presented in Sect. 7.

For any given D, substituting the corresponding $T_{\rm eff}(M_{\rm nucl})$ into $t_{\rm evol}(M_{\rm nucl}, T_{\rm eff})$ yields a $t_{\rm evol}(M_{\rm nucl})$ curve. For $D = 15$ kpc, only large $M_{\rm nucl}$'s can be considered (large L for relatively small $T_{\rm eff}$), so that $t_{\rm evol}$ is necessarily small and meaningless (with our assumptions). For any $D < 12$ kpc, however, the different $t_{\rm evol}(M_{\rm nucl})$ curves almost coincide as long as only relatively small $M_{\rm nucl}$'s are considered. This is because, for the $T_{\rm eff}$'s of interest ($T_{\rm eff} > 1.2\times10^5$ K), $t_{\rm evol}$ depends primarily on $M_{\rm nucl}$, not on $T_{\rm eff}$: $t_{\rm evol}$ increases rapidly as $M_{\rm nucl}$ decreases and, for $M_{\rm nucl} < 0.60\,M_\odot$, the time for the star to climb from 1.2×10^5 K to the maximum $T_{\rm eff}$ is no more than 15−20% of $t_{\rm evol}(M_{\rm nucl})$. For illustration, only one

(approximately) "universal" $t_{\rm evol}(M_{\rm nucl})$ curve is drawn as a solid line labelled "$t_{\rm evol}$" in Fig. 21.

Considering now $M_{\rm nucl}(t_{\rm evol})$, the reciprocal of the previous function, and identifying $t_{\rm evol}$ with $t_{\rm exp}(D, \zeta)$, a function $M_{\rm nucl}(D, \zeta)$ is built; thus, for any given value of ζ, a $M_{\rm nucl}(D)$ or, equivalently, a $D(M_{\rm nucl})$ is obtained. This $D(M_{\rm nucl})$ can be inserted into the function $M_{\rm nucl}(T_{\rm eff}, D)$, and then solved, always for a given ζ, for $T_{\rm eff}(M_{\rm nucl})$: the 3 steep diamond curves in Fig. 21 correspond to $\zeta = 1$, 2, and 3, as labelled. Along any one of these curves, $T_{\rm eff}$ and $M_{\rm nucl}$ are such that the timescales relevant to the shell and the nucleus of PN G135 are both equal to $t_{\rm kin}(D)$, as defined above, but multiplied by ζ. These curves are interrupted at $T_{\rm eff}^{\rm max}/10^5$ K = 1.63, 1.39, and 1.30, for $\zeta = 1$, 2, and 3, respectively. Interpolating in the constant-D (thin solid lines and crosses) and constant-ζ (diamonds) curves, $T_{\rm eff}(M_{\rm nucl})$ curves can be obtained for constant timescales: these are shown in Fig. 21 as thick solid lines for $t_{\rm evol}$ = 6.7, 10, and 15 kyrs, that can be used as consistency check, comparing to Bloecker's tables.

Finally, the six more or less horizontal curves in Fig. 21 indicate lower or upper limits on $T_{\rm eff}$ related to upper limits on the fluxes of undetected emission lines (Sect. 5.7) that proved the most constraining, namely, [Ne IV]$\lambda\lambda$4714+25 (labelled [Ne IV]; flux upper limit 1.5), C IVλ4658 (labelled C IV$_{\rm opt}$; upper limit 1.2), and C IVλ7726 (labelled C IV$_{\rm red}$; upper limit ∼0.12). Both C IV lines are considered, as the far-red line limit is more constraining, but perhaps less well defined. The C1 (C/O = 1.5) and C7 (C/O = 7.3) models shown correspond to non-Case B and data set A, with the C7 models emphasized by asterisks. [Ne IV] (dashed lines) provides lower limits to $T_{\rm eff}$ of order $T_5 > 1.24$, C1 being shifted from C7 by a small δT_5 = +0.018. Concerning C IV, the looser upper limit set by C IV$_{\rm opt}$ is already constraining for C7 models ($T_5 < 1.36$), while the one set by C IV$_{\rm red}$ happens to be *lower* ($T_5 < 1.21$) than even the lower limit set by [Ne IV]. Because the far-red line flux limit is just indicative, the C7 models are not excluded on this basis. In addition plausible variants of C7 models allow to restore strict compatibility between [Ne IV] and C IV$_{\rm red}$ even with these flux limits. Models with covering factor less than unity were already found to present attractive features (Sects. 5.5 and 5.6). Here, assuming $f = 0.5$, the limits set by [Ne IV] and C IV$_{\rm red}$ are shifted by δT_5 = +0.045 and +0.056 respectively (upward arrows in Fig. 21). In another variant, the Ne^{3+} recombination coefficient was, by analogy with recent trends for oxygen, divided by 1.5: then, although C IV is unaffected, the lower limit set by [Ne IV] is shifted down by $\delta T_5 = -0.050$ (downward double arrow). Assuming that both effects are at work, the [Ne IV] curve nearly coincides with the initial one, but, with respect to [Ne IV], the C IV$_{\rm red}$ curve is shifted from $\delta T_5 = -0.035$ up to δT_5 = +0.025, bringing formally the upper limit to $T_{\rm eff}$ above the lower limit. Evidently, the C IV constraint progressively vanishes as smaller C/O values are assumed: in the case of C1, even C IV$_{\rm red}$ will be practically useless (see below). Model variants with pre-Nahar oxygen data (not shown in Fig. 21) lead to insignificant differences for [Ne IV] (δT_5 = +0.01), whereas C IV is shifted by $\delta T_5 \sim +0.08$, thus relaxing the upper limit, but these variants are not very likely (Sect. 6.1.1). From this discussion it can be concluded that the lower limit to $T_{\rm eff}$ imposed by [Ne IV] is a robust one (see also Sect. 6.5).

Summarizing, provided that the evolution of the nucleus of PN G135 follows a standard post-AGB description, *the condition $\zeta > 1$ in Fig. 21 is enough to imply $M_{\rm nucl} < 0.61\,M_\odot$ and, perhaps more interestingly, $D < 10$ kpc (since $T_5 > 1.24$).* J02 argued that D should be much larger than 10 kpc on the basis of a minimum $M_{\rm nucl}$, but the estimate of $M_{\rm nucl}$ from the optical continuum depends on several parameters (Sects. 4.1.1 and 6.5). On the other hand, R02 did not exclude 6.5 kpc, but, because this was out of the scope of their study, they did not favour any D in the range 6.5−25 kpc.

More specifically, for T_5 approaching 1.6, solutions are confined between the minimum $D \sim 6.5$ kpc and the minimum $\zeta \sim 1$ in Fig. 21, so the expansion timescale of the PN tends to $t_{\rm exp}^{\rm min} = 5.2$ kyrs, probably too short to be reconciled with the low density of the nebula. For example, the inner density of PN G135 is ∼1/28 with respect to K 648, suggesting a $t_{\rm exp} \geq 3$ times larger for PN G135, that is, ≥9 kyrs. If a minimum $t_{\rm exp}$ of 8 kyrs is assumed, then $T_5 < 1.47$ and $M_{\rm nucl} < 0.593\,M_\odot$. Accepting $T_5 > 1.4$ implies both $D \sim 7$ kpc and $\zeta \sim 1.8$. If the acceleration of the nebula vanished long ago, one may prefer a smaller ζ, say, $\zeta \sim 1.2$, achievable if $t_{\rm exp} \sim 8.5$ kyrs and $T_5 \sim 1.27$ ($D \sim 9.5$ kpc, $M_{\rm nucl} \sim 0.59\,M_\odot$). However, due to the uncertainties attached to the value of $t_{\rm kin}$, some freedom on ζ is unavoidable. The domain of the ($T_{\rm eff}$, $M_{\rm nucl}$) plane best compatible with timescales and [Ne IV] can be taken as the "trapezium" bounded by the curves $T_{\rm eff} = T_{\rm eff}^{\rm max}$, $T_5 = 1.24$, $t_{\rm evol} = 8$ kyrs and $t_{\rm evol} = 14$ kyrs ($M_{\rm nucl}/M_\odot$= 0.583 ± 0.010, $D/$ kpc $= 8 \pm 1.5$).

Depending on assumptions concerning C/O and the weight given to the C IVλ7726 flux upper limit, the largest acceptable $T_{\rm eff}$ could vary greatly on purely spectroscopic criteria (Sect. 6.1.2). *Timescale considerations now tend to confine the solutions to relatively moderate $T_{\rm eff}$'s ($T_5 = 1.35 \pm 0.11$) for whatever C/O.*

Compared to the standard description adopted so far, the evolution timescale of the PN nucleus may be shortened by the presence of a nearby companion star and lengthened by the occurence of a late He-flash followed by helium burning. In case of He-burning, $t_{\rm evol}$ and therefore $t_{\rm exp}$ can be increased, opening the possibility of larger L, $M_{\rm nucl}$ and D. Assuming schematically that the former $L(M_{\rm nucl}, T_{\rm eff})$ relation still applies and that $t_{\rm evol}(M_{\rm nucl}, T_{\rm eff})$ is uniformly multiplied by a constant factor $K_{\rm ev}$, then Fig. 21 is left unchanged, except in that labels involving $t_{\rm evol}$ should be multiplied by $K_{\rm ev}$. (If, for example, $K_{\rm ev} = 3$, the thick line labelled "6.7 kyrs" should read "20 kyrs", the diamond line "$\zeta = 1$" should read "$\zeta = 3$" and the scale for $t_{\rm evol}/10^3$ to the right should range from 0 to 54). All curves referring to emission lines can be safely prolonged to large $M_{\rm nucl}$'s as straight lines. At $D = 15$ kpc, the mass of a 125 kK black body star will be ∼0.65 $M_\odot$. Adopting a standard $\zeta = 1.5$, the timescale is $t_{\rm evol} \sim 18$ kyrs, that is, very roughly, $K_{\rm ev} = 10$. For lack of a definite law for $t_{\rm evol}$ (or $K_{\rm ev}$), no strong inference concerning L and $M_{\rm nucl}$ can now be made, although the spectroscopic constraints derived from photoionization models and displayed in Fig. 21 are still useful (see also end Sect. 7).

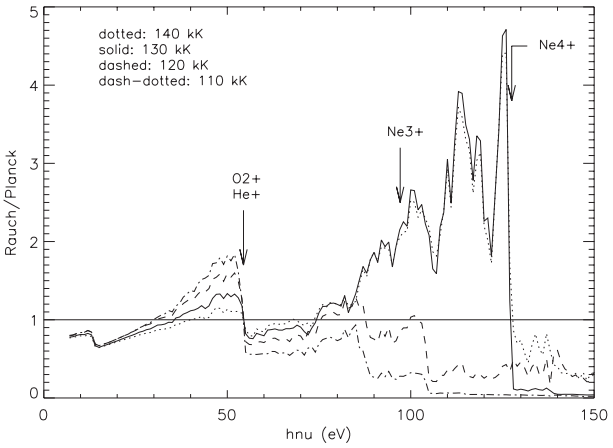

Fig. 22. Stellar atmosphere models (Rauch 2003) for stars with $\log(g) = 6$, $T_{\rm eff} = 110-140$ kK and typical halo chemical composition. Monochromatic fluxes were rebinned over 1 eV intervals and divided by the corresponding flux of the black body at the same temperature. Some ionization limits are indicated.

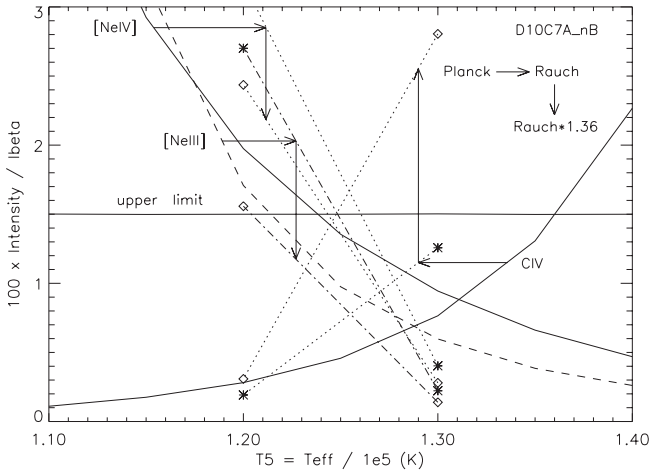

Fig. 23. Predicted line intensities in units $I_{\rm H\beta} = 100$ versus $T_{\rm eff}$ in model sequence D10C7AnB. Solid lines ([Ne IV] and C IV) and dashed lines ([Ne III]): black body stars (as in Fig. 12, but with departure from Case B). Dotted and dash-dotted lines: stellar atmosphere model stars with L either equal to that of the black body (asterisks at $T_5 = 1.2$ and 1.3) or multiplied by a factor 1.36 (diamonds). Horizontal arrows: effect of replacing the black body by the model atmosphere. Vertical arrows: effect of multiplying the model atmosphere fluxes by 1.36.

6.5. Photoionization and stellar atmosphere models

Models so far were obtained assuming that the central star radiated like a black body. This allowed us to generate sequences of models in well-defined conditions, also adopted by R02 and J02.

In Fig. 22 relevant stellar atmosphere spectra computed by Rauch (2003) are shown. Since [Ne IV] plays a critical role in this investigation, the ionization limit of Ne^{3+} (97.1 eV) is indicated. For $T_{\rm eff} = 120$ kK, the normalized flux is about flat (of order unity) until it falls abruptly above $h\nu \sim 106$ eV. For lower $T_{\rm eff}$'s, much fewer photons are left to photoionize Ne^{3+}. For $T_{\rm eff} = 130$ kK on the other hand, the normalized flux increases to high photon energies and the photoionization rate of Ne^{3+} is much larger than with the corresponding black body. The departure from the Planck law is remarkably similar at $T_{\rm eff} = 130$ and 140 kK. Thus, in comparison to black body stars of equal power, model atmosphere stars will lead to under- and over-ionization of Ne^{3+} for $T_{\rm eff}$'s smaller and larger than ∼125 kK respectively.

In the optical, all these model atmospheres have a similar behaviour (Fig. 22), with a flux ∼1.36 times less than for the black body. Since the central star luminosity $L(T_{\rm eff}, D)$ is scaled from the optical flux (Sect. 4.1.1), L should be 1.36 times larger for a model atmosphere star than for a black body star of identical $T_{\rm eff}$. Multiplying L by 1.36 will increase the ionization of Ne^{3+} by a similar amount, while the ionization cascade up to the dominant ions Ne^{4+} or O^{4+}–O^{5+} will affect the ionization of Ne^{2+} or O^{2+} in larger proportions.

Consequences are illustrated in Fig. 23, in which predicted [Ne III], [Ne IV] and C IV intensities are displayed versus $T_5 = T_{\rm eff}/10^5$ K for three different central star continua: (1) black body as previously; (2) model atmosphere with L as for the black body; and (3) model atmosphere with L multiplied by the factor 1.36. Since interpolation at $T_5 = 1.25$ would be risky in this highly non-linear regime, model atmospheres are only considered for $T_5 = 1.2$ and 1.3 and the results are linked by straight lines. The [Ne IV] intensity is predicted twice stronger

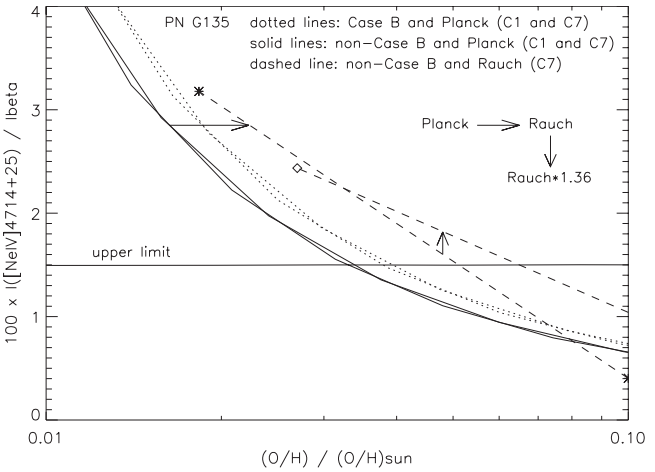

Fig. 24. Predicted intensity of multiplet [Ne IV] versus O/H in solar units. Dotted and solid lines as in Fig. 14 (black body stars). Dashed lines and arrows: stellar atmosphere model stars as in Fig. 23.

at $T_5 = 1.2$ and twice weaker at $T_5 = 1.3$ after replacing the black body by the stellar atmosphere and [Ne IV] is weaker after multiplying L by 1.36. The [Ne III] intensity is less sensitive to changes of the primary spectrum itself, but is more affected by the increase of L, particularly at $T_5 = 1.3$. Correlatively, since the [O III] intensity must be accounted for, the oxygen abundance is increased, which reflects, for given C/O, in the marked increase of the predicted C IV intensity.

Thus, owing to the highly non-linear behaviour of the stellar atmosphere models in this particular range of temperatures, the variation of the computed intensities with $T_{\rm eff}$ is much steeper than for a black body. Needless to insist that values of $T_{\rm eff}$ below 120 kK are much more violently excluded than in the previous black body analysis. Interestingly, while

Table 3. Models for PN G135 and comparison to K 648.

Model	M 1	M 2	M 3	M 4	K 648
Dist. D/ kpc	6.5	8.0	8.0	10.0	12.0
$T_{\rm eff}/10^5$ K	1.42	1.30	1.30	1.20	0.425
$L/10^{37}$ erg/s	0.88	1.03	1.39	1.73	2.80
Log (g)	6.42	6.19	6.06	5.83	3.82
Spectrum	BB	BB	R	R	R
$Q_H/10^{47}$ ph/s	1.38	1.70	2.14	2.87	2.95
Cov. factor f	0.75	1.0	1.0	1.0	.9+.1
n_c/ cm^3	294	234	235	211	6000
$\langle N_{\rm e}\rangle$/ cm^3	74	59	59	53	1300
$T_{\rm e}^{\rm inner}/10^4$ K	3.5	3.7	3.4	3.9	1.2
$\langle T_{\rm e}\rangle/10^4$ K	2.9	3.0	3.0	3.0	1.3
$\tau_{13.6}$	.030	.025	.025	.026	.4−.8
$R_{\rm neb}/10^{17}$ cm	4.8	5.9	5.9	7.4	2.7−3.2
$M_{\rm neb}/10^{-2}\,M_\odot$	2.5	4.9	4.9	8.6	11.6
$I({\rm H}\beta)^a$	2.7	2.7	2.7	2.7	103.4
$M_{\rm nucl}/\,M_\odot$	.588	.583	.591	.600	.61
$t_{\rm evol}/10^3$ yrs	9.5	11.0	8.8	6.6	3.0
$\zeta = t_{\rm evol}/t_{\rm kin}$	1.83	1.72	1.36	0.82	–
Abundances by number:					
H	1.00	1.00	1.00	1.00	1.00
He	.0813	.0809	.0813	.0818	.082
C ($\times10^6$)^b	100.	84.0	82.5	98.5	280.
N ($\times10^6$)^c	20.0	6.3	27.5	5.0	14.3
O ($\times10^6$)	38.5	21.0	55.	13.5	38.5
Ne ($\times10^6$)	4.66	4.45	3.38	5.13	6.80
Mg ($\times10^6$)^c	0.20	0.20	0.20	0.20	0.30^c
S ($\times10^6$)^c	0.05	0.03	0.06	0.03	0.04:
Ar ($\times10^6$)^b	.009	.006	.012	.005	0.01:
Fe ($\times10^6$)^b	.033	.030	.020	.033	–

[a] In units of 10^{-14} erg cm^{-2} s^{-1}.
[b] Upper limit.
[c] Arbitrary value.

Table 4. Observations and model predictions for PN G135.

Ident.	(Å)	Obs.	Err.	M 1	M 2	M 3	M 4
Hβ	4861	100.	–	100.	100.	100.	100.
Hα	6563	281.	±14.	288.	289.	290.	289.
Hγ	4340	45.5	±1.	45.0	44.5	44.4	44.5
Hδ^a	4102	25.6	±1.5	20.0	19.7	19.6	19.6
H7^a	3970	13.0	±2.	11.8	11.7	11.6	11.6
[Ne III]	3968	bl.	–	0.08	0.16	0.03	0.37
H8^a	3889	9.4	±2.	7.6	7.6	7.5	7.5
He I	3889	bl.	–	.052	.060	.048	.076
He I	5876	<.3	–	.044	.050	.040	.063
He I	7065	<.1	–	.015	.017	.014	.022
He I	1.1 μ	–	–	0.19	0.20	0.16	0.24
He II	4686	83.2	±1.5	83.2	83.2	83.2	83.2
He II	5412	6.79	±.4	6.75	6.75	6.75	6.75
C IV	4658	<1.	–	0.33	0.27	0.27	0.31
C IV	7726	<.12	–	0.14	0.12	0.12	0.14
[N II]	6584	<.4	–	.004	.002	.002	.001
N V	4945	<1.	–	.045	.010	.087	.004
[O II]	3727	<2.	–	.004	.004	.003	.004
[O III]	5007	2.9	±.8	2.90	2.90	2.90	2.90
[O III]	4363	<.9	–	.157	.161	.165	.162
O IV	4632	<1.	–	.068	.037	.097	.024
O IV	7713	<.1	–	.025	.013	.035	.009
O V	4930	<1.	–	.017	.005	.035	.001
O V	7611	<.1	–	.007	.002	.015	.000
[Ne III]	3869	1.07	±.5	0.26	0.52	0.11	1.19
[Ne IV]	4715	<1.	–	0.27	0.45	0.15	0.93
[Ne IV]	4725	<1.	–	0.44	0.73	0.24	1.50
[Ne V]	3426	82.2	±8.	82.2	82.2	82.2	82.2
[S III]	9069	<.08	–	.004	.006	.003	.007
[Ar III]	7136	<.06	–	.001	.002	.001	.002
[Ar IV]	4711	<1.	–	.021	.031	.020	.043
[Ar IV]	4740	<1.	–	.017	.025	.017	.034
[Ar V]	7006	<.09	–	.087	.091	.087	.093
[Fe VI]	5146	<.7	–	.074	.123	.036	.040
[Fe VII]	6087	<.5	–	0.49	0.50	0.48	0.50
O VI	1034	–	–	256.	92.	619.	15.
N V	1240	–	–	749.	306.	922.	279.
O IV]	1401	–	–	77.	66.	94.	55.
N IV]	1487	–	–	137.	77.	120.	78.
C IV	1549	–	–	1100	1320	912.	1980
C III]	1908	–	–	28.	38.	18.	50.
[Ne IV]	2423	–	–	31.	50.	16.	102.
[Mg V]	2783	–	–	2.	2.	1.	2.
[O IV]	26 μ	–	–	64.	52.	65.	55.
[Ne V]	14 μ	–	–	50.	47.	46.	44.
[Ne V]	24 μ	–	–	57.	53.	52.	50.
[Ne VI]	7.6 μ	–	–	18.	9.	1.	2.

[a] No collisional excitation included in models.

the detectability of the [Ne IV] lines will be very significantly reduced for large $T_{\rm eff}$'s, the minimum T_5 consistent with the upper limit to the [Ne IV] intensity is almost the same, namely, $T_5 \sim 1.24$, for all three assumptions (Fig. 23). Thus, *the fundamental* [Ne IV] *boundary in the ($M_{\rm nucl}/M_\odot$, $T_{\rm eff}$) diagram of Fig. 21 is left unchanged* when model atmospheres are used, although it is sharper, hence more significant.

Figure 24 illustrates another important aspect of using model atmospheres. The predicted [Ne IV] intensity at given value of O/H tends to be larger than using a black body and the effect is more pronounced after applying the scaling factor 1.36 to the star luminosity. It follows that *the minimum acceptable oxygen abundance is significantly larger than in the previous black body analysis*, being shifted from $[{\rm O/H}]_{\rm min} = -1.5$ to:

$$[{\rm O/H}]^{\rm atmos}_{\rm min} \sim -1.3,$$

now only 0.2 dex less than in K 648.

In Fig. 23, the narrow range of possible $T_{\rm eff}$'s that was available for C7 models (C/O = 7.3) between the antagonistic limits set by [Ne IV] and C IV is reduced to literaly one unique point at $T_5 = 1.24$ when model atmospheres are used (dotted lines connecting diamonds). No solution would be left if the more stringent far-red C IV line upper limit were considered. The upper limit to C/O is now ∼5 by number instead of 10 (Sect. 6.1.2).

On replacing black bodies by model atmospheres, previous results can apply to a first approximation, provided that a model with $T_{\rm eff}$ multiplied by a factor $\sim 1.36^{1/4} = 1.08$, typically $\Delta T_5 = 0.05-0.10$, is picked up from the existing

sequences. Thus, as suggested by Fig. 24, using stellar atmospheres instead of black bodies, larger O/H's are obtained at given $T_{\rm eff}$ (Fig. 5). However, further distortions can be induced by the $T_{\rm eff}$-dependent departure from the black body, notably around 125 kK (Fig. 22).

Consequences of considering stellar atmospheres in Fig. 21 can be summarized as follows. Firstly, curves referring only to stellar evolution and nebula kinematics (thick solid lines, diamonds, crosses) are left unchanged. Secondly, the important [Ne IV] lower limit was demonstrated to be left unchanged (the C IV upper limits are not significantly changed either). Thirdly, due to the factor 1.36 rise of $L(T_{\rm eff}, D)$, constant-D loci (thin solid curves labelled in kpc in Fig. 21) are shifted *down* by ~8 kK with some distortions. In particular, the distance approximately associated to $T_{\rm eff}^{\rm max}$ decreases from $D_{\rm min}^{\rm BB} \sim 6.5$ to $D_{\rm min}^{\rm Rauch} \sim 5.5$ kpc.

7. "Best model" for PN G135

Four photoionization models, M 1 to M 4, are described in Table 3 and compared to an unpublished model for K 648 (last column). These models are represented by filled stars in Fig. 21. All of them are built using the best standard data, notably the Anderson et al. (2002)'s collision strengths for H I, and allowing for departure from Case B. The central star spectrum is a black body for M 1 and M 2 and a stellar atmosphere model (Rauch 2003) for M 3 and M 4. Note the low density and the small optical depth $\tau_{13.6}$ of PN G135. In the upper part of Table 3, $M_{\rm nucl}$, $t_{\rm evol}$ and ζ depend somewhat on the adopted stellar evolution model, that is, on the ill-defined status of the progenitor star. In the lower part, not all abundances given have the same meaning: while H, He, O and Ne are effectively determined, C, Ar and Fe are upper limits, whereas N, Mg and S are arbitrary guesses. (Concerning K 648, C and N are determined, whereas S and Ar are poorly determined).

In Table 4, the model predictions (Cols. 5−8) are compared to the observations (Cols. 3−4) for the emission lines listed in Cols. 1−2. Many line intensities in Col. 3 are just 2-σ upper limits and most of these are ineffective, given the weakness of the predicted intensities. Exceptions are C IV, [Ne IV], [Ar V] and [Fe VII]. Concerning [Ne IV], the upper limit 1.5 was for the sum of the multiplet in previous sections: equivalently, in Table 4, this limit is set to 1.0 for each multiplet component.

Observed line intensities are well accounted for in all models, except for Hδ and, with lesser significance, H7 and H8. Unlike for the first Balmer lines, no trustworthy collisional excitation rates are available for these lines. Effective collision strengths Ω_n are presented in Table 5 for transitions $1s \rightarrow n$, $n \leq 8$ at $T_{\rm e} \sim 30$ kK. In Table 5, the 1st row lists the Case B intensity I_n and the 2nd row the relative enhancement $\Delta I_n/I_n$ due to collisional excitation (and cascades). $\Delta I_n/I_n$ is obtained from the model computation for $n \leq 5$ and from observation for $n > 5$. The indication here is that, in the exceptionnally hot plasma of PN G135, *the fraction of the excitation rate of Hδ due to electron collisions is at least as large as for Hγ*. The 3rd row lists Ω_n, taken from Anderson et al. for $n \leq 5$ and derived empirically from $\Delta I_n/I_n$ for $n > 5$. Finally the 4th row is a smooth law ($\propto n^{-2.44}$) to be compared to the 3rd row. The empirical Ω_n's are roughly consistent with the smooth extrapolation within errors, but with a hint that Ω_6 is larger and perhaps Ω_7 smaller. When these empirical collision strengths are introduced in the models, the excitation of the first Balmer lines is slightly enhanced by cascades and the model abundances of He, O and Ne are increased by 1.3, 2.8 and 1.4% respectively.

Table 5. Collision strengths Ω_n from level $1s$ of hydrogen.

n	3	4	5	6	7	8
I_n/I_4^a	270	100	47.8	26.6	16.4	10.8
$\Delta I_n/I_n^b$	16.0	13.5	14.1	30 ± 8	11 ± 17	24 ± 26
Ω_n^c	330	150	95	95 ± 26	23 ± 36	20 ± 22
$\propto n^{-2.44}$	330	163	95	61	42	30

[a] Case B Balmer decrement $\times 10^2$.
[b] Relative collisional enhancement $\times 10^2$.
[c] Effective collision strength $\times 10^3$ ($T_{\rm e} \sim 30$ kK).

Considering first the models with black-body central stars, Model M 1 is designed to have the same O/H as K 648. $T_{\rm eff}$ must be relatively large and M 1 lies close to the upper corner of the trapezoidal domain defined in the ($T_{\rm eff}$, $M_{\rm nucl}$) plane at the end of Sect. 6.4, with the distance D at its minimum of 6.5 kpc. Taking the far-red C IV line upper limit at face value, C/O is at most one third of its value in K 648. The mass of the shell, small as a consequence of the small D, is further lowered by the use of a covering factor $f < 1$, allowing to keep the value of He/H above 0.081, as it should (Sect. 5.6.1). Since Model M 1 appears acceptable in all respects, *PN G135 is not firmly established as the most oxygen-poor PN known*. Note that the very small mass $M_{\rm neb}$ of the nebula in Model M 1 is not intrinsic to the assumption of a relatively large O/H: adopting $D = 8$ kpc, $M_{\rm neb}$ is ~0.041 $M_\odot$ and $t_{\rm evol}$ just slightly short (~7.5 kyrs).

With an intermediate D and a moderate $T_{\rm eff}$, Model M 2 lies close to the barycentre of the trapezium and, as such, can be taken as a kind of a "standard solution", as long as *black body* stars are used. In Model M 2, O/H is 1.8 times less than in K 648.

Model M 3 is a D8C1AnB model, but with an atmosphere model central star. M 3 can be directly compared to M 2 (same D and $T_{\rm eff}$), illustrating the influence of the primary spectrum. Due to the larger L, $M_{\rm nucl}$ is slightly larger and Model M 3 lies off the curve "8 kpc" in Fig. 21, as explained in Sect. 6.5. Strikingly, O/H is multiplied by a factor 2.6, being now 1.4 times *larger* than in K 648, and the maximum C/O set by C IV$_{\rm red}$ is reaching the minimum value of 1.5 that was thought worthwhile to consider. If so, Model M 3 also illustrates the maximum acceptable O/H, while Ne/O ~ 0.06 is near its minimum value. Given the available data and our current state of knowledge, notably the unreliable 2-σ detection of [Ne III] (Sects. 3.1 and 3.2.1), it is difficult to point out any feature of Model M 3, that would allow us to strongly argue against this solution. However, the observed intensity of [Ne III], if it were confirmed to order of magnitude, *would very seriously challenge Model M 3 and its "extreme"* O/H (Table 4).

Model M 4, a D10C7AnB model at the lower right corner of the trapezium, illustrates at once the tremendous influence of $T_{\rm eff}$ on the predicted spectrum of PN G135 when stellar atmosphere models are used in this range of temperature and the consequence of adopting a relatively large D. With ΔT_5 only −0.1 relative to M 3, [Ne IV] is predicted 6 times stronger and O VI 40 times weaker in M 4. With $T_{\rm eff}$ just slightly less than the established minimum, O/H is particularly low, in fact *too low* since the upper limit to [Ne IV] is already by-passed by a factor 1.5 (Table 4). Nonetheless, playing with the uncertainty on $\alpha(Ne^{3+})$, marginal consistency with this upper limit could be restored (Sect. 6.1.1). At 10 kpc, the mass of the nebula is approaching the one of K 648 but both $t_{\rm evol}$ and ζ violate their probable lower limits. Thanks to the low $T_{\rm eff}$, C/O can be as large as in K 648, but PN G135 and K 648 are still far from being twins, with the O/H's now differing by a factor of almost 3.

The neon abundance is systematically and significantly less in PN G135 than in K 648, but the factor ∼2/3 difference is moderate, given the scatter of Ne/H among the GHPNe. The maximum carbon abundance in most models of PN G135 is of order 1/3 the abundance in K 648, but this result depends on the adopted upper limit to the intensity of C IVλ 7726. Based on C IVλ 4658, a larger C/H is still possible in PN G135. In all models shown, the helium abundance is near to 0.081 (0.082 with empirical Ω's of Table 5), but it must be noted that He/H is among the non-spectroscopic criteria used in the selection of an acceptable model (Sect. 5.6.1). The important point is that models with He/H in agreement with expectation are naturally obtained using the a priori best physical description.

These models illustrate and re-inforce the conclusions of the extensive study of PN G135 conducted in previous sections. They also provide line intensity predictions that can help selecting a definite model from new observations. Both Models M 3 and M 4 may be slightly too extreme in some respects. Due to the very fast rise of O/H from 120 to 130 kK when stellar atmospheres are used, $T_{\rm eff}$'s in excess of 130 kK are unlikely, unless an unexpectedly small C/O (and Ne/O) is adopted for PN G135. Thus, if some credit is given to the recent stellar atmosphere models of Rauch (2003), it should be concluded that possible $T_{\rm eff}$'s for PN G135 are confined to an extremely narrow range, say, 124−128 kK. Changing, e.g., the chemical composition of the model atmosphere does not change fundamentally the emergent spectrum. The effect of a stellar wind is more difficult to quantify, but may be moderate in this low-Z star. If the truth lies somewhere in between the Planck and Rauch descriptions, yet closer to the latter, some flexibility concerning $T_{\rm eff}$ is recovered. A $T_{\rm eff}$ slightly less than 130 kK and [O/H] = −1.2 provide a likely combination. Taking into account inferences of Sects. 6.4–6.5, the distance to PN G135 is 6−9 kpc, with D = 8 kpc a good value. Then, $M_{\rm nucl}$ is 0.59 $M_\odot$ ($L = 1.4\times10^{37}$ erg s^{-1}) and $t_{\rm evol}$ is slightly less than 10 kyrs, i.e., 1.5 times the kinematic timescale of the PN, in excellent agreement with the value advocated by Gesicki & Zijlstra (2000) on empirical grounds. A best set of abundances by number for PN G135 is: (H:He:C:O:Ne) = (10^6:81 500:90:30:4.5), in which C/H is rather an upper limit, N/H is omitted for lack of constraints and, *allowing for substantial departure from the standard description*, e.g., in the oxygen and neon ionization, O/H is uncertain by 0.3 dex (formal uncertainty 0.2 dex) and Ne/H by 0.1 dex.

If no definite evolution timescale is available to link $M_{\rm nucl}$ to the size of the nebula, D and L are free. For larger D and $M_{\rm nucl}$, the lower limit to $T_{\rm eff}$ is very slightly relaxed (Fig. 21) and the model elemental abundances follow a similar trend. In Model M 2, transposed from 8 to 15 kpc (with L multiplied by a factor 3.5, etc.), O/H is multiplied by a factor 1.9 and the intensity predicted for C IVλ 7726 is increased by a similar factor. In order to strictly fulfill the C IV upper limit, a smaller C/O should be adopted. Alternatively, adopting T_5 = 1.24 instead of 1.30, the oxygen abundance of M 2 is recovered. Nonetheless, in these new models at 15 kpc, the derived helium abundance is some 5% less. The preferred He/H (Sect. 5.6) can be recovered by considering a covering factor less than unity, which in turn leads to a much lower O/H (Fig. 5). After full reconvergence, it turns out that the original $T_{\rm eff}$, O/H and He/H of M 2 apply to first order at 15 kpc, but with a smaller covering factor. These comments illustrate how dependent on conditions the model abundances are. They also illustrate how the spectroscopic constraints, when they are considered consistently in the model, tend to confine the acceptable values within a small interval.

8. Conclusions and possible status of PN G135

The low abundance of the heavy elements, the very high ionization related to the low electron density and the high effective temperature $T_{\rm eff}$ of the star all concur to bring the electron temperature $T_{\rm e}$ of PN G135 up to 3×10^4 K, an unprecedented value for a galactic photoionized nebula. The collisional excitation of the H I Balmer lines is considerable, providing a unique opportunity to check existing collisional rates from the ground state of H^0. Out of three representative data sets considered, only the one of Anderson et al. (2002) is fully satisfactory from the standpoints of both the Balmer decrement and the helium abundance determination, leading, at $T_{\rm e}$ = 30 kK, to collisional excitations of levels n = 3−5 roughly proportional to the respective recombination excitations. No collisional data are available for levels $n > 5$. Observation of PN G135 indicates that the fraction of the excitation of these levels due to collisions is again about the same as for Hβ and Hγ.

While it is known that the carbon and nitrogen content of PNe is strongly influenced by the progenitor nucleosynthesis, it is still widely believed that oxygen is essentially preserved at least for low-mass progenitors, despite a growing body of observational and theoretical indications, particularly for (low-mass) low-Z stars (Sect. 2.2.1). The conclusion of R02 and J02 that O/H is one to two orders of magnitude lower in PN G135 than in any other PN known would constitute, if it were accepted, a crucial first example of a low-metallicity PN deprived of endogenous oxygen in significant amount. However, the strength of [Ne V]λ 3425 would then imply an amazingly large Ne/O and the upper limit to the intensity of [Ne IV]λ 4715+24 would be violated. Based on the non-detection of [Ne IV] and extensive photoionization model analysis, a *very robust* lower limit to the oxygen abundance turns out to be [O/H] > −1.5. Hence, with a high degree of confidence, [O/Fe] > 1 in

PN G135 and the inference of Sect. 2.2.1 concerning K 648 can be directly transposed: it is likely that a large fraction of oxygen (and neon) present in PN G135 was synthesized, dredged-up and ejected by its progenitor star. Accretion of nucleosynthetically processed gas from a hypothetical former AGB companion could be an alternative, but this would simply confirm that copious amounts of oxygen are brought to the surface during the third dredge-up in very metal-poor AGB stars.

On the other hand, timescale considerations indicate that the mass of the nucleus of PN G135 is probably $\sim 0.59\,M_\odot$ and that [O/H] < -1 is a reasonably safe upper limit, also consistent with the upper limit to the intensity of the C IV lines and a minimum C/O ratio of 1.5 by number, very likely for this low-mass low-Z progenitor. While it is probably true that PN G135 is a new member of the highly select club of GHPNe with [O/H] < -1, it is not yet certain that PN G135 has the lowest [O/H].

Out of the three previously known members of the club (Peña et al. 1991; Peña et al. 1993; Howard et al. 1997), one, M 2−29, presents large S and Ar abundances and is probably not an extreme Pop II object (also, its carbon abundance is unknown). Both remaining GHPNe, K 648 and BB-1, present exceedingly large C/O ratios and, in that respect, seem to differ from PN G135. Alves et al. (2000) suggest that *all* extreme Pop II PNe originate in the late common-envelope evolution of close binary stars. In this scenario, the very large C/O might be a consequence of the strong mixing accompanying the interaction. That very peculiar mixing occured in the precursors of these PNe is most obvious in the case of BB-1, in which the Ne/O ratio is ∼1 by number. The case for a close binary precursor to K 648 is especially attractive although no companion could so far be found, suggesting that the binary system ended in a coalescence (Alves et al. 2000).

Although the statistics are poor and the upper limit to C/H in PN G135 is still fragile, this difference in carbon abundance may give credit to the suggestion that PN G135 originated in a different process. Could it be a single, extremely metal-poor, star (Sects. 2.1 and 2.2.2)? Using a diagram provided by Willson et al. (1996) or Fig. 9 in Willson (2000)'s review [with the concept of a "cliff" replaced by one of an "overhang": see Fig. 7 of that review], a "metal-free" star of initial mass $0.75\,M_\odot$ experiencing a dredge-up bringing the heavy element content of its envelope up to $Z/Z_\odot = 0.12$ (best model of Sect. 7) will precipitously expel $\sim 0.15\,M_\odot$, ending as a remnant of mass $0.595\,M_\odot$ and luminosity 1.44×10^{37} erg s^{-1}. This rapid estimate is in suggestive agreement with the conclusions of Sect. 7. However, for such a low-mass star, the more likely elements to be produced and dredged up would be CN rather than ONe, even in case the core He-flash-induced mixing (Fujimoto et al. 2000) could be inhibited. Thus, a close binary precursor may again provide a more attractive explanation. The apparently less extreme mixing in PN G135 than in K 648 (and BB-1) may suggest that the common-envelope interaction has not been so strong in PN G135.

The fact that the upper limit to the metallicity of PN G135 ([Fe/H] < -2.5; Sect. 6.2) is significantly less than the metallicity of K 648 ([Fe/H] $= -2.26$ in M 15) and BB-1 ([Fe/H] ~ -2 from [Ar/H]) indicates that the progenitor of PN G135 belongs to a more primordial population. The status of PN G135 depends much on its metallicity, which can be best, though indirectly, diagnosed by means of [Ar V]. It is therefore desirable to obtain *extremely deep far-red spectra* of PN G135 in order to significantly improve the detection limit of [Ar V]. Detecting [Fe VII] itself would obviously be of great interest too since it would provide a lower limit to the metallicity.

Determining as accurately as possible a lower limit to [O/H] in PNe is of paramount importance to guide stellar evolution theory. What makes PN G135 a fundamental object is its low oxygen abundance. If this abundance is certainly not as extreme as previously claimed, PN G135 is still a candidate to supplant K 648 as the most oxygen-poor PN known. In order to establish this with any confidence, it is again necessary to secure very deep optical and far-red spectra, that will bring stronger constraints on the intensities of [Ne III], [Ne IV], C IV, along the lines developed in this study, and new no less useful direct constraints on oxygen and nitrogen recombination lines.

Note added in proof. Two months after submitting this manuscript, we became aware of the serendipitous (and stupendous) discovery by Tovmassian et al. (2004, hereafter T04) that the nucleus of PN G135 (PNN) belongs to a binary system whose period is no more than a few hours. T04 confirm our inference that the nebular Balmer decrement is influenced by underlying stellar absorption (Sect. 3.2.2). From Balmer absorption line profiles, T04 derive a relatively small $\log(g)$, hence a large luminosity for the hot central star (now assumed much hotter than in R02 and J02, and thus in better agreement with present findings), and finally a distance ∼18 kpc, two times larger than our derived value. Nonetheless, as admitted by T04, their description of the binary system is far from satisfactory in several respects, including (1) an amazingly massive PNN for a Pop II system and (2) an impossibly small separation of the stellar components prior to the common-envelope (CE) phase, which presumably led to the PN ejection.

In order to alleviate the problem of the PNN mass, T04 suggest that the stellar radius and, particularly, the luminosity may be unusualy large, due to a late He-flash ("born-again scenario", e.g., Iben 1995). Nonetheless, if transitory luminosity excesses are indeed predicted by stellar evolution models in this process, the standard luminosity tends to be recovered, as the star reaches again high $T_{\rm eff}$ in its second journey to the WD stage (the luminosity of He-burners can actually be somewhat less).

Assuming that only the hot PNN contributes to the optical stellar emission and that its mass is $0.55\,M_\odot$, T04 infer that the companion star should be a massive WD, raising the question of how the system became a PN, as opposed to some cataclysmic variable or soft X-ray source. T04 exclude that the companion star is a low-mass main-sequence star by analogy with other binary systems, such as BE UMa. Nonetheless, given the large luminosity of the PNN and, particularly, the small separation of the components, the photosphere of a "main-sequence" companion could be so hot as to emit a spectrum totally different from the one of BE UMa.

If the companion contributes to the emission, the interpretation of the radial velocity oscillations would not be straightforward and the observed small $\log(g)$ would not necessarily correspond to the PNN alone. Playing with the observational uncertainty on radial velocities and, e.g., the inclination of the binary, solutions could be explored in which the mass of the PNN is $\sim 0.6\,M_\odot$, the mass of the companion is smaller and its radius larger, possibly approaching its Roche lobe size, given the short time since the CE phase resumed. The picture could then suggest that a bona fide low-mass cataclysmic variable is just newly born. On replacing the black body by a Rauch model atmosphere, the luminosity $L(T_{\rm eff})$ of the PNN must be larger (Sect. 6.5). If, on the other hand, the companion contributes to the optical continuum, $L(T_{\rm eff})$ may decrease back to the black body value or even below (Sect. 4.1.1). A definite description of the binary system is needed.

Acknowledgements. We are grateful to the referee, Dr. Albert Zijlstra, for valuable suggestions.

References

Aggarwal, K. M. 1983, MNRAS, 202, 15
Aggarwal, K. M., Berrington, K. A., Burke, P. G., Kingston, A. E., & Pathak, A. 1991, J. Phys. B, 24, 1385
Anders, E., & Grevesse, N. 1989, Geochimica et Cosmochimica Acta, 53, 197
Anderson, H., Ballance, C. P., Badnell, N. R., & Summers, H. P. 2000, J. Phys. B, 33, 1255
Anderson, H., Ballance, C. P., Badnell, N. R., & Summers, H. P. 2002, J. Phys. B, 35, 1613 (Erratum)
Allende Prieto, C., Lambert, D. L., & Asplund, M. 2001, ApJ, 556, L63
Alves, D. R., Bond, H. E., & Livio, M. 2000, AJ, 120, 2044
Argast, D., Samland, M., Gerhard, O. E., & Thielemann, F.-K. 2000, A&A, 356, 873
Asplund, M., Grevesse, N., Sauval, A. J., Allende Prieto, C., & Kiselman, D. 2004, A&A, 417, 751
Barker, T. 1980, ApJ, 237, 482
Barker, T. 1983, ApJ, 270, 641
Beers, T. C. 1990, AJ, 99, 323
Bensby, T., Feltzing, S., & Lundström, I. 2004, A&A, 415, 155
Bloecker, T. 1995, A&A, 299, 755
Boothroyd, A. I., & Sackmann, I.-J. 1988, ApJ, 328, 671
Bowen, G. H., & Willson, L. A. 1991, ApJ, 375, L53
Callaway, J. 1994, ADNDT, 57, 9
Castellani, V. 2000, in The first stars, ESO Astrophys. Symp., ed. A. Weiss, T. Abel, V. Hill (Springer), 85
Cayrel, R., Depagne, E., Spite, M., et al. 2004, A&A, 416, 1117
Chiosi, C. 2000, in The first stars, ESO Astrophys. Symp., ed. A. Weiss, T. Abel, V. Hill (Springer), 95
Christlieb, N., Gustafsson, B., Korn, A. J., et al. 2004, ApJ, 603, 708
de Marchi, G., Paresce, F., Straniero, O., & Prada Moroni, P. G. 2004, A&A, 415, 971
Dinerstein, H. L., Richter, M. J., Lacy, J. H., & Sellgren, K. 2003, AJ, 125, 265
Drake, S. A., & Ulrich, R. K. 1980, ApJS, 42, 351
Edelmann, H., Heber, U., Hagen, H.-J., et al. 2003, A&A, 400, 939
Fujimoto, M. Y., Ikeda, Y., & Iben, I., Jr. 2000, ApJ, 529, 25
Garnett, D. R., & Lacy, J. H. 1993, ApJ, 419, L93
Gesicki, K., & Zijlstra, A. A. 2000, A&A, 358, 1058
Giovanardi, C., Natta, A., & Palla, F. 1987, A&AS, 70, 269
Grebel, E. K. 2000, in Star formation from the small to the large scale, ed. F. Favata, A. Kaas, & A. Wilson, ESA SP, 445, 87
Habing, H. J., Tignon, J., & Tielens, A. G. G. M. 1994, A&A, 286, 523
Harris, W. E. 1996, AJ 112, 1487
Herwig, F. 2000, A&A, 360, 952
Hippelein, H., & Weinberger, R. 1990, A&A, 232, 129
Howard, J. W., Henry, R. B. C., & McCartney, S. 1997, MNRAS, 284, 465
Hummer, D. G., & Storey, P. J. 1992, MNRAS, 254, 277
Ibata, R. A., Wyse, R. F. G., Gilmore, G., Irwin, M. J., & Suntzeff, N. B. 1997, AJ, 113, 643
Iben, I., Jr., 1995, Phys. Rev., 250, 2
Iben, I., Jr., 1999, Asymptotic Giant Branch Stars, ed. T. Le Bertre, A. Lèbre and C. Waelkens (Kluwer), IAU Symp., 191, 591
Iben, I., Jr., & Livio, M. 1993, PASP, 105, 1373
Iben, I., Jr., & Renzini, A. 1983, ARA&A, 21, 271
Iben, I., Jr., & Tutukov, A. V. 1993, ApJ, 418, 343
Izotov, Y. I., Chaffee, F. H., Foltz, C. B., et al. 1999, ApJ, 527, 527
Izotov, Y. I., & Thuan, T. X. 1999, ApJ, 511, 639
Jacoby, G. H., Feldmeier, J. J., Claver, C. F., et al. 2002, AJ, 124, 3340 (J02)
Jacoby, G. H., Morse, J. A., Fullton, L. K., Kwitter, K. B., & Henry, R. B. C. 1997, AJ, 114, 2611
Johnson, L. C. 1972, ApJ, 174, 227
Kingsburgh, R. L., & Barlow, M. J. 1994, MNRAS, 271, 257
Kisielius, R., & Storey, P. J. 2002, A&A, 387, 1135
Koesterke, L., & Hamann, W.-R. 1997, Planetary Nebulae, ed. H. J. Habing and H. J. G. L. M. Lamers (Kluwer), IAU Symp., 180, 114
Krolik, J. H., & McKee, C. F. 1978, ApJS, 37, 459
Kudritzki, R.-P., & Puls, J. 2000, ARA&A, 38, 613
Lattanzio, J. C. 1989, ApJ, 344, L25
Livio, M., & Soker, N. 1988, ApJ, 329, 764
Luridiana, V., Peimbert, A., Peimbert, M., & Cerviño 2003, ApJ, 592, 846
Marigo, P. 2001, A&A, 370, 194
Marigo, P., Girardi, L., Chiosi, C., & Wood, P. R. 2001, A&A, 371, 152
Marsteller, B., Beers, T. C., Rossi, S. et al. 2003, AAS Meet., 203, 112.16
McCarthy, J. K., Mould, J. R., Mendez, R. H., et al. 1990, ApJ, 351, 230
Mendoza, C. 1983, Planetary Nebulae, ed. D. Flower (Reidel), IAU Symp., 103, 143
Nahar, S. N. 1999, ApJS, 120, 131
Nahar, S. N., & Pradhan, A. K. 1997, ApJS, 111, 339
Nissen, P. E., Primas, F., Asplund, M., & Lambert, D. L. 2002, A&A, 390, 235
Nussbaumer, H., & Storey, P. J. 1984, A&AS, 56, 293
Peña, M., Torres-Peimbert, S., & Ruiz, M. T. 1991, PASP, 103, 865
Peña, M., Torres-Peimbert, S., Peimbert, M., & Dufour, R. J. 1993, Rev. Mex. Astron. Astrofis., 27, 175
Péquignot, D., Ferland, G., Netzer, H., et al. 2001, in Spectroscopic Challenges of Photoionized Plasmas, ed. G. Ferland & D. W. Savin, ASP Conf. Ser., 247, 533
Péquignot, D., Petitjean, P., & Boisson, C. 1991, A&A, 251, 680
Péquignot, D., Walsh, J. R., Zijlstra, A. A., & Dudziak, G. 2000, A&A, 361, L1
Rauch, T. 2003, A&A, 403, 709
Rauch, T., Heber, U., & Werner, K. 2002, A&A, 381, 1007
Renzini, A., & Fusi Pecci, F. 1988, ARA&A, 26, 199
Richer, M. G., Lopez, J. A., Steffen, W., et al. 2003, A&A, 410, 911

Richer, M. G., Tovmassian, G., Stasińska, G., et al. 2002, A&A, 395, 929 (R02)
Richer, H. B., Fahlman, G. G., Ibata, R. A. et al. 1997, ApJ, 484, 741
Rola, C., & Pelat, D. 1994, A&A, 287, 676
Rossi, S., Beers, T., Sneden, C. 1999, in: The Galactic Halo, ed. Gibson, B. K., Axelrod, T. S. & Putman, M. E., ASP Conf. Ser. 165, 264
Ryde, N., & Lambert, D. L. 2004, A&A, 415, 559
Schlattl, H., Cassisi, S., Salaris, M., & Weiss, A. 2001, ApJ, 559, 1082
Schlattl, H., Salaris, M., Cassisi, S., & Weiss, A. 2002, A&A, 395, 77
Schlegel, D. J., Finkbeiner, D. P., & Davis, M. 1998, ApJ, 500, 525
Siess, L., Livio, M., & Lattanzio, J. 2002, ApJ, 570, 329
Sivarani, T., Bonifacio, P., Molaro, P., et al. 2004, A&A, 413, 1073
Storey, P. J., & Hummer, D. G. 1995, MNRAS, 272, 41
Torres-Peimbert, S., Rayo, J. F., & Peimbert, M. 1981, Rev. Mex. Astron. Astrofis., 6, 351
Tovmassian, G. H., Stasińska, G., Chavushyan, V. H., et al. 2001, A&A, 370, 456
Tovmassian, G. H., Stasińska, G., Chavushyan, V. H., et al. 2002, RMxAC, 12, 146
Tovmassian, G. H., Napiwotzki, R., Richer, M. G., et al. 2004, [arXiv:astro-ph/0407518/v1] (23 Jul. 2004) (T04)
Umeda, H., & Nomoto, K. 2003, Nature, 422, 871
VandenBerg, D. A., Swenson, F. J., Rogers, F. J., Iglesias, C. A., & Alexander, D. R. 2000, ApJ, 532, 430
VandenBerg, D. A., Richard, O., Michaud, G., & Richer, J. 2002, ApJ, 571, 487
Willson, L. A. 2000, ARA&A, 38, 573
Willson, L. A., Bowen, G. H., & Struck, C. 1996, in From stars to galaxies: the impact of stellar physics on galaxy evolution, ed. C. Leitherer, U. Fritze-von-Alvensleben, and J. Huchra, ASP Conf. Ser., 98, 197
Woosley, S. E., & Weaver, T. A. 1995, ApJS, 101, 181
Zijlstra, A. A. 2004, MNRAS, 348, L23
Zijlstra, A. A., & Walsh, J. R. 1996, A&A, 312, 21